RESISTANCE OPTIMIZATION FOR SKELETAL MUSCLE DURING EXERCISE

by

Matthew Edwards

A thesis submitted to the faculty of
The University of North Carolina at Charlotte
in partial fulfillment of the requirements
for the degree of Master of Science in
Mechanical Engineering

Charlotte

2015

Approved by:

_____
Dr. Nigel Zheng

_____
Dr. Ron Smelser

_____
Dr. Mesbah Uddin

_____
Dr. Erik Wikstrom

ABSTRACT

MATTHEW ARTHUR EDWARDS. Resistance optimization for skeletal muscle during exercise. (Under the direction of DR. NIGEL ZHENG)

The physical fitness industry is booming due to an increase in health awareness. People are spending more time and money to become healthy and stay healthy. Physical exercise has been proven to improve mental and physical health, but what if we are going about it all wrong?

The goal of this study is to prove that current forms of exercise do not work skeletal muscle to its full capability and to gain evidence for the design of exercise equipment that will exercise skeletal muscle more effectively. Three common exercises using a free weight and strength bands were evaluated for how well they exercise the elbow flexors. Static optimization was performed in order to determine the effectiveness of the free weight and strength band. This study shows that current exercises do not work muscles to their full potential.

Motion capture data was taken of a subject performing the exercises and then imported into OpenSim for further analysis. Customized static optimization was performed based on the physiological parameters of skeletal muscle in order to calculate the muscle forces during the exercise. The results show that the elbow flexors were activated as low as 12.6% at the beginning of the exercise and as high as 100% at the end. The findings of this study will have an impact on rehabilitation therapy, surgical programs, and athletic training programs, as well as, provide insight into the design of an optimized moment of resistance for skeletal muscle.

ACKNOWLEDGEMENTS

I would like to thank all of my family for their constant love and support. My educational career would have been considerably harder without them. I would also like to thank Dr. Nigel Zheng for all of his help and guidance throughout this project, as well as, Dr. Ronald Smelser, Dr. Mesbah Uddin, and Dr. Erik Wikstrom for serving on my thesis committee. I also want to thank Dr. Scott Delp and the OpenSim team at Stanford University for the creation of OpenSim.

TABLE OF CONTENTS

CHAPTER 1: INTRODUCTION

People are becoming more aware of the effects that their diet and exercise have on their well-being. An effect of this is a rise in demand to be healthy and fit. A study done by the University of Washington's Institute for Health Metrics and Evaluation (IHME) reported that physical activity in the United States is increasing. In the most active U.S. counties, the number of people exercising sufficiently rose by up to 17 percent for males and 18 percent for females from 2001 to 2009 (Dwyer-Lindgren et al. 2013). Due to the increase in physical activity, the fitness industry is booming. The International Health, Racquet, and Sports Association (IHRSA) reported that the total revenue in the fitness industry increased from $20.3 billion in 2010 to $21.8 billion in 2012, IHRSA (2013), and exercise equipment sales have grown in fitness centers from $484 million in 1996 to $1.3 billion in 2013 (Statista.com 2015). To put it simply, people are spending more time and money to stay physically fit and healthy.

How do consumers know that they are exercising their muscles properly? What if current exercises and machines do not work our muscles to their full potential? Can better exercise equipment be designed to shorten workouts while improving workout quality? If exercise equipment could be designed to maximize workout efficiency, it would revolutionize the fitness world and usher in an entirely new generation of fitness products. Better designed workout equipment would save the user time and work the muscles more effectively. So, what do we need to determine how effective a workout is?

One way is to calculate the muscle forces that drive the motion. In order to design better exercise equipment, it is crucial to understand muscle function during an exercise or motion. Once the basic functions of muscle force generation are understood, that knowledge can be used to take advantage of muscle function during an exercise.

Every muscle is attached at one end to a bone, crosses a joint, and attaches to another bone. When the muscle contracts, the bones rotate around the joint. When we exercise, our muscles generate force by contracting while working against an external resistance. When the muscle contracts, it produces a force that pulls on the bone in order to produce joint movement. Knowledge of muscle forces and their action is essential in order to understand how we are working our muscles during an exercise. If muscle forces can be determined, this information can be used in many different applications. For example, physical therapists and athletic trainers are always looking for the safest and most effective exercises for their patients. The muscle forces during a given exercise can be used to determine how effective and safe that exercise is, as well as, to provide insight in the design of better exercise machines. Muscle force calculation can be of equal benefit to much more than the design of exercise equipment. Athletes can use it to analyze their techniques during movement or when performing a task-specific exercise in order to achieve exceptional performance. Motion capture systems have been used to analyze golf swings (Zheng et al. 2008) and pitching form (Aguinaldo et al. 2007). The kinematics of these motions are useful when calculating the muscle forces that generate movement of the skeletal system (Escamilla et al. 2001), (Escamilla et al. 2009). The muscle forces during movement can also be beneficial to surgeons and surgical programs. Changing the insertion point of a muscle has a drastic effect on that muscle's function. A

surgeon wishes to know how their operation is going to affect their patient's movement. Overall, muscle force generation is at the heart of all human body movement, and the quantification of it can lead to endless possibilities.

The goal of this study is to prove that current exercises do not work our muscles effectively and gain evidence towards the design of equipment that works them to their full capability. Current exercises have low resistance when the muscles are at their strongest and high resistance when muscles are at their weakest. Half of the exercise is wasted motion because the muscle's potential force is so high and the resistance is so low. The aim is not to work the muscle to 100% of its maximum potential with every repetition. The aim is to work the muscles to a desired percentage of their maximum potential during the entire exercise.

Muscles have a maximum potential force that they can generate. However, it is not constant as a muscle contracts. Maximum muscle potential changes along with the length of the muscle and the speed of contraction. The goal is to take advantage of this by applying more resistance at certain points in the exercise when the muscles are at their strongest and reducing the resistance at points when the muscles are weaker. For this purpose, the elbow flexor's muscle forces were calculated using static optimization during three different types of curl exercises. The elbow joint was chosen due to its simplicity and availability of information concerning the elbow flexors and the upper extremity. There was no need to model a complicated motion or joint, such as the shoulder, because all skeletal muscles generate force the same way. The exerted torque at the elbow is mainly a result of the force produced by the three elbow flexors: biceps brachii (BIC), brachialis (BRA), and brachioradialis (BRD) can be seen in Figure 1. This

system of muscle and bone can be analyzed as a mechanical system. The muscles provide an active force acting on the forearm which is a lever.

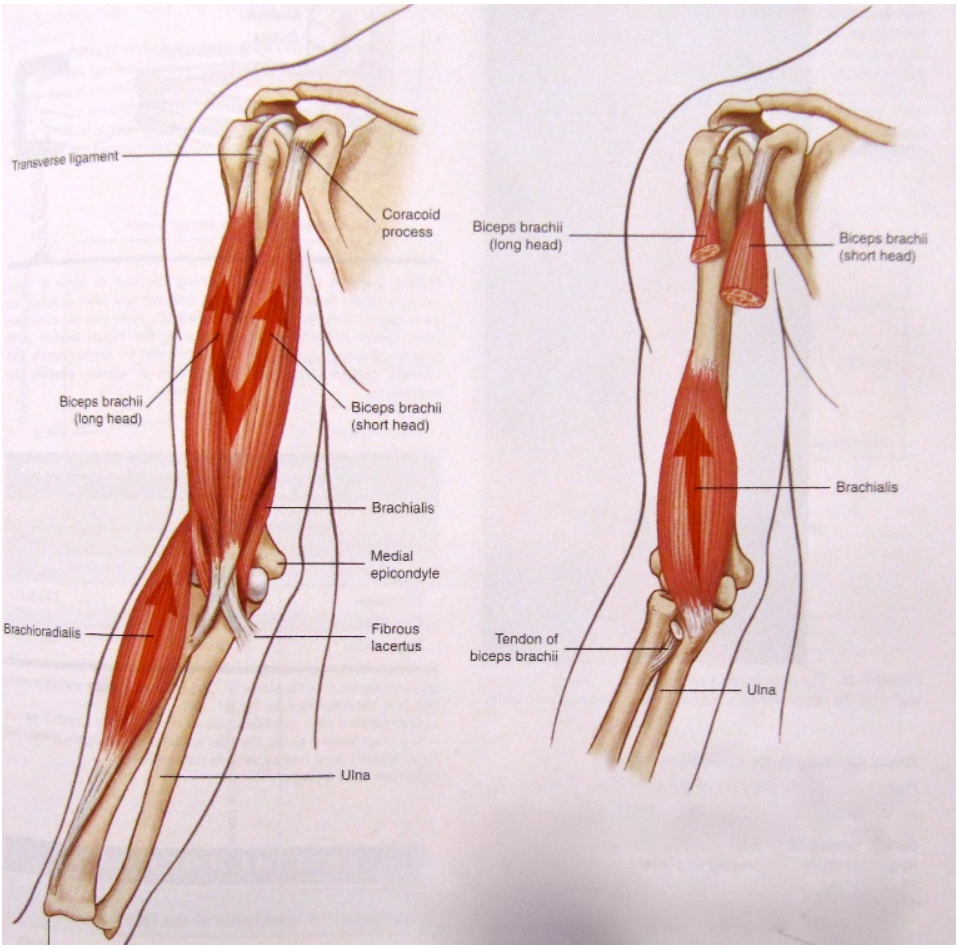

Figure 1: Diagram of the elbow flexors, (Neumann 2002).

The curl is a popular exercise to strengthen the elbow flexors, and it is effective in isolating the them. This exercise consists of the subject holding a form of resistance in their hand while contracting the elbow flexors. The starting position, in general, is when the elbow is at 0° of flexion. Next, the subject contracts the elbow flexors, bringing the hand closer to the shoulder. The curl motion can be seen in Figure 2. There are different variations of the curl which will be discussed later in this study. The two most popular forms of resistance are the free weight (dumbbell) and an elastic band (strength band).

Figure 2 is an example of someone using a strength band. The ways in which they are used and how they work the elbow flexors will be discussed later in Chapter VI. This thesis will show that current forms of resistance do not take advantage of potential muscle force throughout the entire range of motion, calculate the optimized resistance during the full range of motion, and provide insight towards the design of better exercise equipment.

Figure 2: Example of someone using a strength band.

CHAPTER 2: MUSCLE ARCHITECTURE AND PHYSIOLOGY

2.1 The Oxford Dictionary defines muscle as a band or bundle of fibrous tissue in a human or animal body that has the ability to contract, producing movement in or maintaining the position of parts of the body. There are three different types of muscle. These are cardiac, smooth, and skeletal. Cardiac muscle is found only in the heart and has very high endurance and consistency. Smooth muscle is in the blood vessels, digestive system, and air ways. It is controlled involuntarily by the brain and has the ability to stretch and maintain tension for long durations. Skeletal muscles perform a variety of different functions in the body including the movement of the skeletal system, assisting in joint stability, and maintaining posture and body positioning. Skeletal muscles are the muscles that body builders increase in size for competitions. They are the muscles we exercise during a workout.

To understand muscle force, it is helpful to understand how the muscle is organized and activated from the microscopic level to the macroscopic level. To begin, a muscle is made up of thousands of muscle cells or muscle fiber. A picture of a muscle cell can be seen in Figure 3.

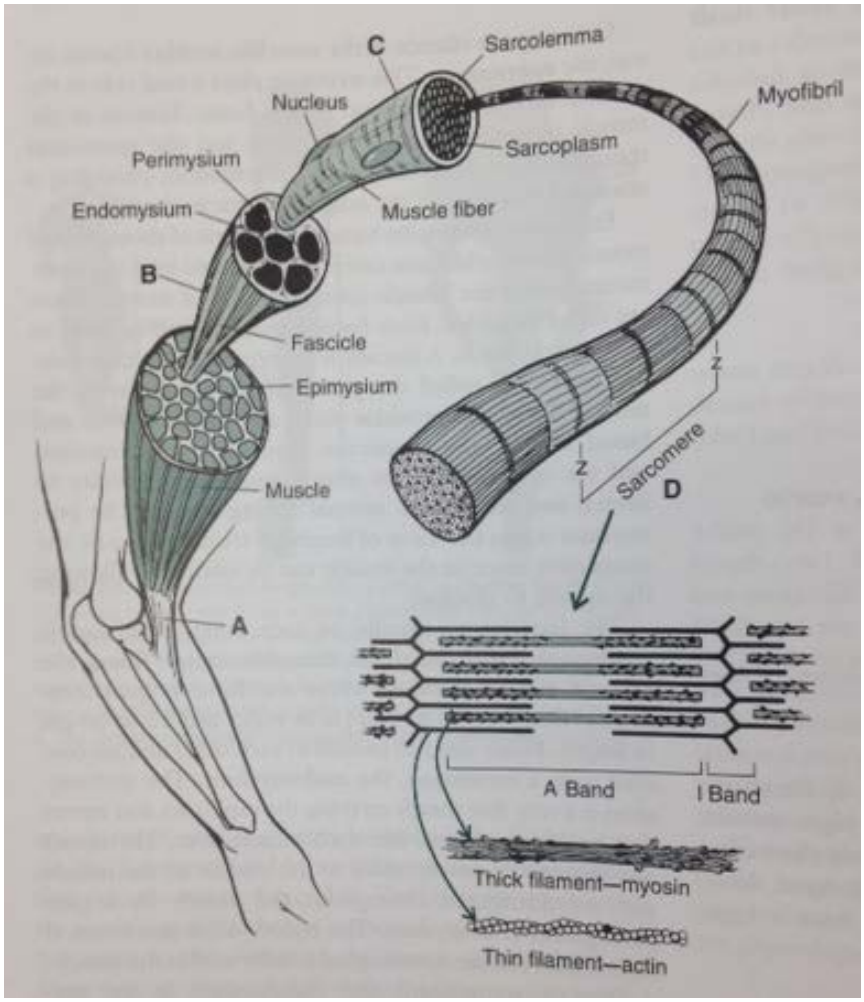

Figure 3: The anatomy of the muscle cell, (Hamill and Knutzen 2009).

A muscle fiber can be thought of as a long thin cylinder. The contraction of the individual muscle fibers will result in the contraction of the entire muscle. Each muscle cell has two types of filament inside: myofibril and actin. These two filaments do the work to contract the cell. During contraction, the myosin attaches to the actin filament and forms a cross bridge. Then the myosin pulls the actin past it, therefore, shortening the cell. Muscles create force by cycling myosin cross bridges. The cross bridges are broken and reformed over and over again throughout the contraction of a muscle. Figure 4 shows the basic setup of the myosin and actin inside of the sarcomere.

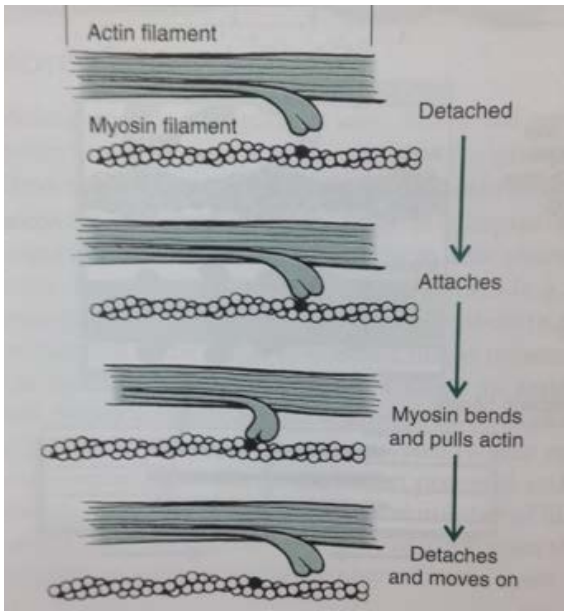

Figure 4: Diagram of the myosin (thick filament) and actin (thin filament) binding sites. Myosin forms a cross bridge at the Actin binding sites (Troponin) and pulls the Actin filament past it, shortening the sarcomere, (Hamill and Knutzen 2009).

The cross bridges or activation sites are of critical importance to how much force the muscle can produce. The more activation sites that are available means the more potential force a muscle can generate. It can be thought of as pulling a rope. The more hands that are grabbing the rope means the more potential force with which the rope can be pulled. How does this process begin? The contractions of all muscles are triggered by an electrical impulse. The impulse can come from nerve cells, created internally as with a pacemaker, or applied externally as with an electrical shock. The electrical impulse, no matter where it comes from, causes a chemical reaction which triggers the myosin cycling process. Voluntary muscle contraction is the result of an electrical impulse, or action potential, being sent from the spinal cord, down the nerve axon, and to the group of muscle fibers. The action potential can be measured with the use of electromyography (EMG).

2.2. A group of muscle fibers belongs to a single motor unit. Every group of muscle fiber is supplied by one nerve fiber, or axon, which is connected to the spinal cord and delivers the action potential. A single motor unit consists of a group of muscle fibers, the spinal cord, and the body of nerve cells which connect them (Figure 5). The contraction of a skeletal muscle is the result of many motor units firing at one time.

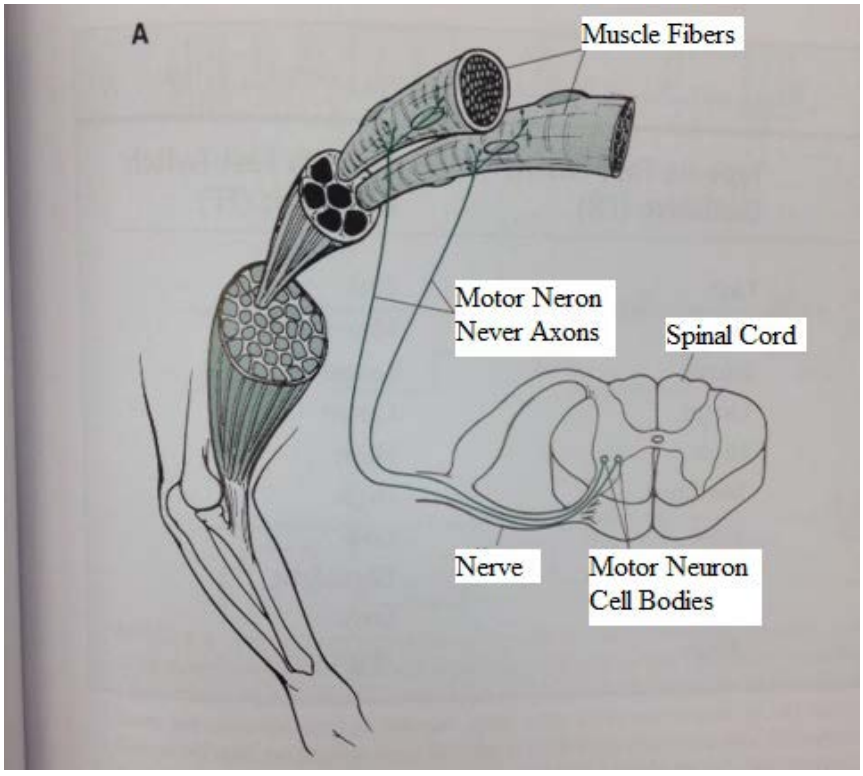

Figure 5: The motor unit, (Hamill and Knutzen 2009).

To summarize muscle contraction, an action potential is sent from the spinal cord, down the nerve axon, to a group of muscle fibers. The action potential activates the chemical (ATP) process in the muscle fibers which causes the myosin cycling process. During the myosin cycling process, myosin forms cross bridges with actin and slides the actin past it, therefore, shortening the muscle cell and generating force. This is the fundamental process of how the muscle turns energy into force.

2.3. As mentioned before, the available myosin and actin binding sites are of the upmost importance. There is an optimal fiber length at which the maximum amount of binding sites are available. If the muscle is stretched beyond this point, actin is pulled past the myosin and results in less binding sites. If the muscle is shortened beyond the optimal fiber length, the actin sites start to overlap resulting in less binding sites. Either way, if the muscle is not at optimal fiber length, it will have less potential force. This relationship is known as the length-force relationship**.** Skeletal muscles reach their peak force values when the sarcomere is at a length of 2.8 μm (Buchanan et al. 2004, Holzbaur et al. 2005). At this length, we say that the fiber is at optimal muscle fiber length, l_o^m. However, this occurs at different muscle lengths for different muscles. It is helpful to take the length-force curve described by Gordon et al. (1966) and normalize it (Figure 6**).** This curve has been modeled as a second-order polynomial by Woittiez et al. (1984), but it is more accurate to model it as a cubic polynomial (An et al. 1989, Buchanan et al. 2004).

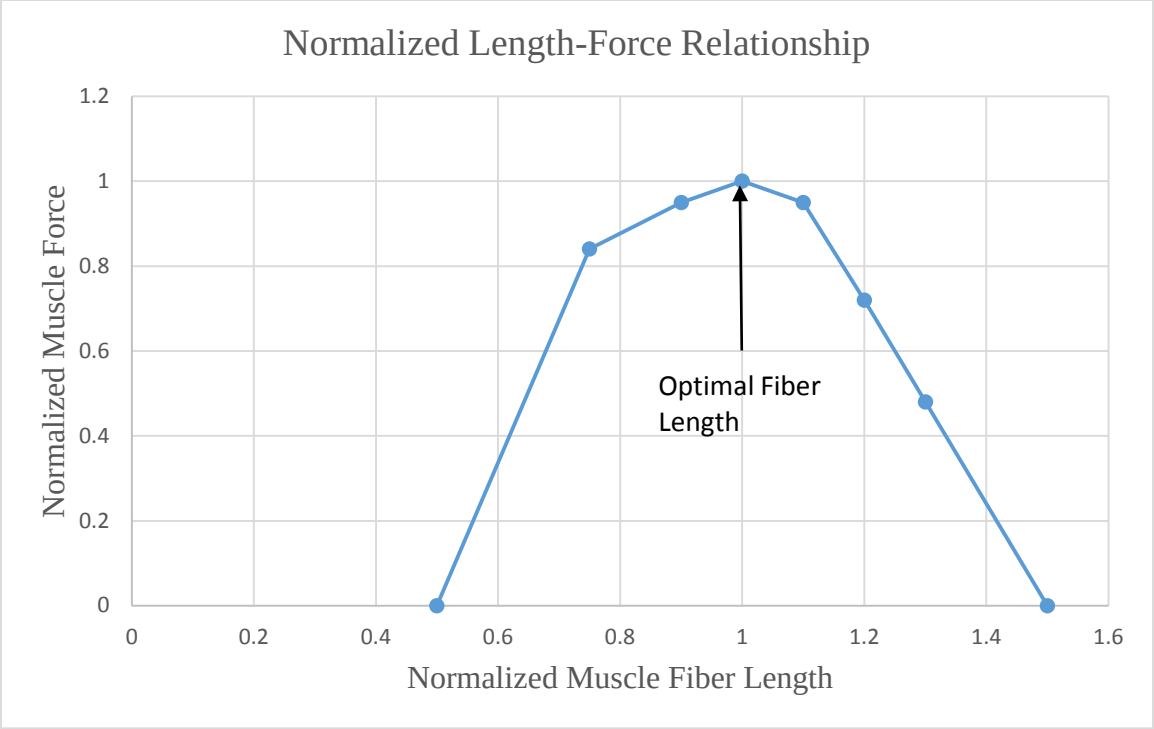

Figure 6: Normalized length-force relationship for muscle. Resting length is optimal muscle fiber length, edited from Buchanan et al. (2004).

Optimal fiber lengths are reported in Table 1. These values were reported by Holzbaur et al. (2005) and were used by Saul et al. (2014) in the creation of a dynamic arm model.

Table 1: *LH-long head. *SH-short head.

	BIC LH*	BIC SH*	BRA	BRD
Optimal Fiber Length (cm)	11.6	13.2	8.6	17.3

2.4. The muscle force potential is also dependent on the velocity of muscle contraction. During a concentric contraction, muscle force potential decreases as the velocity of contraction increases, Figure 8. As the velocity of muscle shortening increases, the cycling rate of the cross-bridges increases which decreases the number of cross-bridges attached at one time. Fewer cross-bridges means a lower force potential. It is helpful to think about the rope example again. Picture a rope moving past you. The

faster the rope is being pulled, the less chance that there is to get a good grip on it and get a forceful pull. Maximum muscle force was calculated assuming optimal contraction velocity.

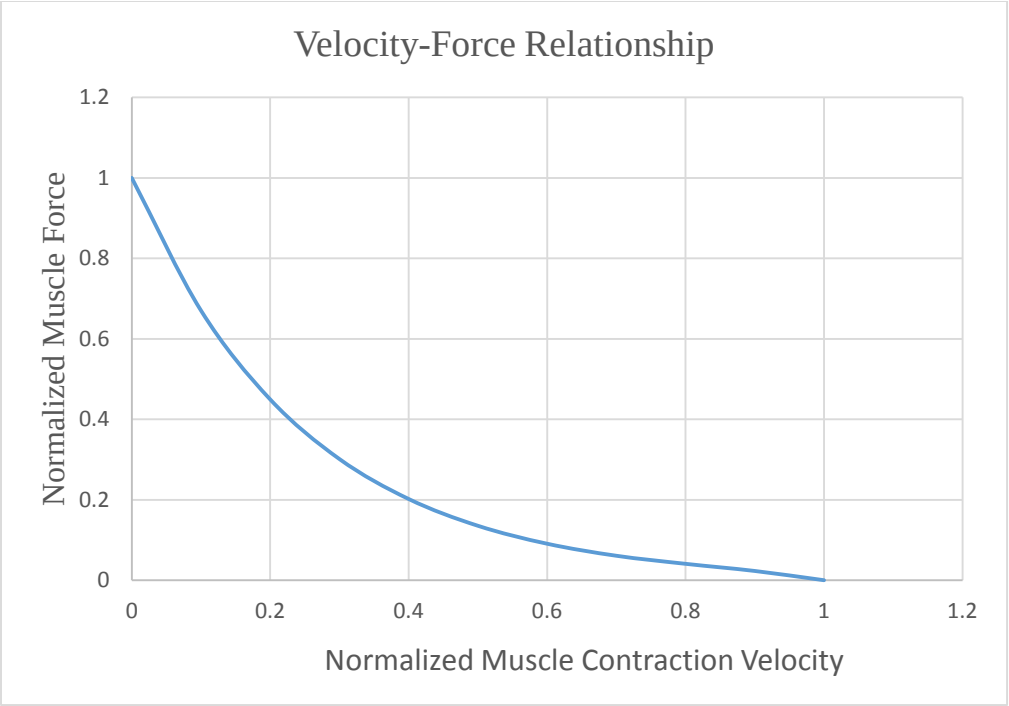

Figure 8: Velocity-force relationship.

2.5. Although muscles produce linear force, motions at joints are all rotary. The contraction of a muscle will produce a moment about the joint. The moment arm is the perpendicular distance from the axis of rotation to the line of action of the force. Therefore, the torque that can be produced at a joint at any given time is dependent on the sum of the muscle forces and their moment arms. The moment created by an individual muscle can be calculated using

$$T = F_m \bullet r \quad . \tag{1}$$

Here T is the torque generated by the muscle, F_m is the muscle force, and r is the muscle's moment arm. More torque can be generated with a larger moment arm given the same muscle force. A muscle's moment arm changes during joint movement. At 0° of flexion, the moment arms of the three muscles are very small. At 90° of elbow flexion, the moment arm of the three muscles are larger than at 0° of flexion. The changes and effects that the moment arm has on joint torque will be discussed in more detail in Chapter 6. Figure 9 shows a picture of the moment arm.

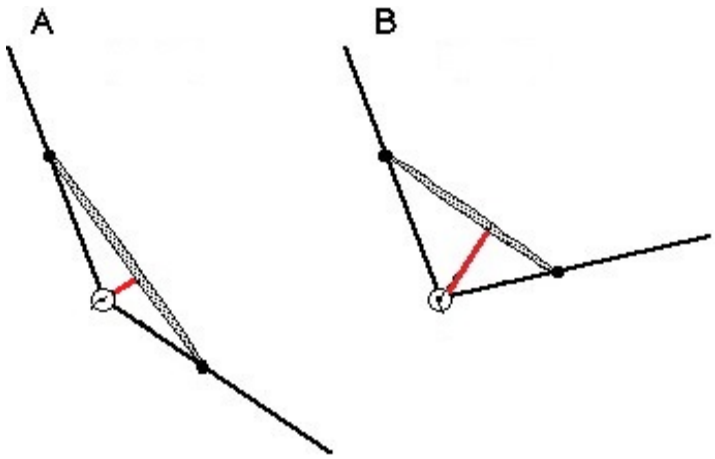

Figure 9: Diagram of how the moment arm (red line) changes during flexion.

2.6. There are other factors that affect a muscle's ability to generate force. The arrangement of muscle fibers has an effect on how much force will be exerted at the tendon's insertion point. Two major fiber arrangement types are parallel and pennate and can be seen in Figure 10.

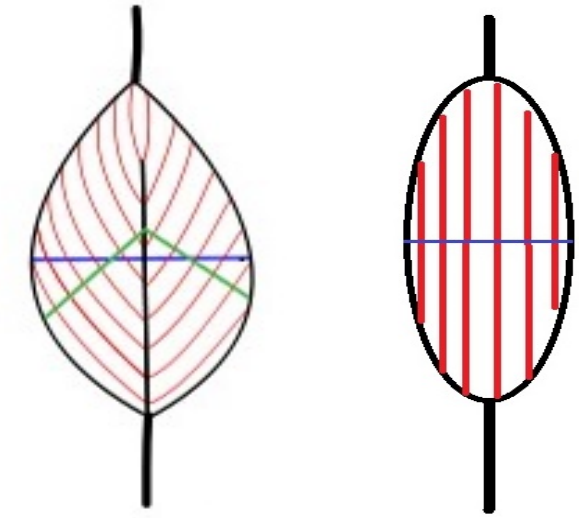

Figure 10: Left- Example of a pennate muscle (Deltoid). The blue line represents the CSA, and the green line represents the PCSA. Right- Example of a parallel muscle (BIC). The blue line represents the CSA.

In a parallel fiber arrangement, the muscle fibers pull parallel to the long axis of the muscle. In other words, the muscle fibers pull in the same direction as the line of action of the muscle. Examples of this type of muscle are the elbow flexors and the obliques. In a pennate fiber arrangement, muscle fibers run diagonally with respect to a central tendon. A good comparison to a pennate muscle would be a feather. Because the fibers do not run parallel to the tendon, the force of the fiber does not pull in the same direction as the muscle's line of action. An example of a pennate muscle is the deltoid. The angle at which the fibers pull on the long axis of the muscle is called the pennation angle. A large pennation angle will decrease the amount of potential force a muscle can produce along its line of action. The arrangement of the muscle fibers will also affect how much stress the muscle can handle. The stress is calculated as

$$\sigma = \frac{F}{A} \quad . \tag{2}$$

Here is the stress measured in $N \cdot cm^{-2}$, F is the tension in the muscle, and A is the muscle's cross sectional area (CSA). Values for have been reported to be anywhere from 20-140 $N \cdot cm^{-2}$. Based on An et al. (1989), Li et al. (2006), and Chang et al. (1999), 100 $N \cdot cm^{-2}$ is the reasonable value. It should be noted that a muscle's CSA changes during flexion. Thus, changing the maximum allowable tension in the muscle. This will become important when adding constraints to the muscle model. The muscle's CSA is calculated from

$$CSA = \frac{V}{L_m} \quad . \tag{3}$$

Here V is the muscle volume and L_m is the length of the muscle. As the muscle contracts, the CSA increases since the muscle volume stays the same. The BIC is made up of two muscles: BIC long head and BIC short head. The BIC long head crosses the shoulder and has a different attachment point on the shoulder. The BIC short head attaches at the top of the arm. Towards the elbow, both muscles merge into the same tendon. The CSA of the BIC was calculated by adding the CSA of the long head to the short head.

Typically, a bigger muscle volume means that there are more muscle fibers. More muscle fibers means that more force can be generated. Muscle volumes have been reported by Holzbaur et al. (2007) by taking the average of five healthy, male muscle volumes and can be seen in Table 2. The muscle volumes chosen for this study are from the same specimens that were used to create the dynamic simulation model in OpenSim. The peak isometric forces used in this study were from the same specimens that the muscle volumes were taken from. These values do not agree with muscle volumes

reported by An et al. (1981). However, high variability in muscular parameters is expected (Murray et al. 2000). The muscular parameters from the study conducted by An et al. (1981) could just as easily be used because those values could represent any number of people in the world.

Table 2: Average muscle volume of five average sized male cadavers

	BIC	BRA	BRD
Volume $[cm^3]$	143.7	143.7	65.1

Overall, with respect to muscle physiology and architecture, muscle forces were calculated in this study considerating the length-force relationship, CSA, muscle volume, and moment arm of each muscle. According to Murray et al. (2000), these are all key factors that characterize the moment generating capacity of the joint. When all of these parameters are taken into account, the calculation of the muscle forces will be more realistic than modelling the muscle as an external force alone. Numerous other studies have been reviewed, but none have modeled the muscle using all of these parameters during an entire range of motion with the addition of an external load.

CHAPTER 3. MODELING AND CALCULATING MUSCLE FORCE

3.1. There are two main models used for calculating muscle force: Huxley-type and Hill-type. The Huxley-type model focuses on the muscle on a microscopic scale. Huxley's model is used to calculate the force generated by individual cross-bridges in a single muscle fiber. There are hundreds of thousands of muscle fibers in a whole muscle making the Huxley model extremely complex.

Many researchers who do large-scale muscle force computation use Hill-type models. This model was developed by Hill (1938) and was used by Kaufman et al. (1991), Millard et al. (2013), and Lemay and Crago (1996) in the creation of computational musculotendon models. It has also been validated by Biewener et al. (2014) to predict muscle forces in vivo. An advantage of the Hill-type model is that it characterizes the external behavior of the muscle rather than looking at the underlying anatomical make-up of a muscle. This model has significant advantage over the Huxley-type model because its dynamics are governed by one differential equation per muscle. This makes the model more computationally viable and the preferred choice when calculating muscle force. The governing equation for the Hill-type model is Equation 4.

$$(F + a)\left(v + \frac{a \bullet v_o}{F_o}\right) = (F_o + a)\left(\frac{a \bullet v_o}{F_o}\right) \quad (4)$$

Here F_o is the maximum isometric force, F is the tension in the muscle, v is the velocity of contraction, v_o is the maximum velocity of contraction, and a is the coefficient of shortening heat.

Another attractive factor that the Hill-type model has is that the muscular parameters can be scaled to match important physiological parameters of any muscle (Millard et al. 2013). The Hill-type muscle model has three components shown in Figure 11**.** The active component of the system is the muscle. It is modeled in parallel with the passive component of the muscle which is the force due to the muscle's elastic nature. The active component is also modeled in series with an elastic component (tendon). In this study, the tendon is assumed to be a rigid component due to its relatively high stiffness.

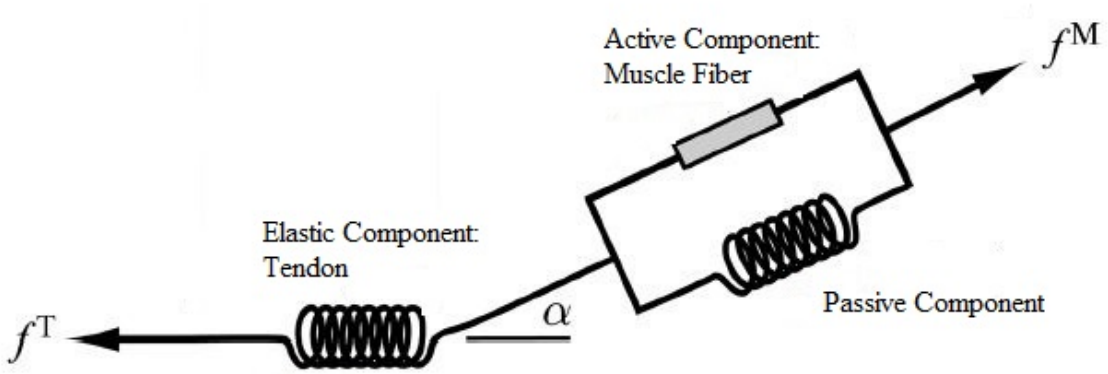

Figure 11: Three component system. Elastic Component-Tendon modeled in series with 2 parallel components. Active component- Muscle fiber. Passive component – force due to muscle elasticity. is the pennation angle (Millard et al. 2013).

The Hill-type muscle model is used to determine the active component's force during an exercise. The maximum muscle (active) force at any point in time can be calculated from Equation 5, (Buchanan et al. 2004).

$$F^m = f(v)f(l)aF_o^m \tag{5}$$

where F^m is the maximum muscle fiber force at a given muscle length, $f(v)$ is the normalized velocity dependent fiber force, $f(l)$ is the normalized length dependent fiber force, a is the activation level, and F_o^m is the maximum isometric muscle fiber force. The maximum isometric forces of the muscles have been reported by Saul et al. (2014), Table 3.

Table 3: Max isometric force of the elbow flexors.

	BIC LH	BIC SH	BRA	BRD
Maximum Isometric Force [N]	525.1	316.8	1177.4	276.0

$f(v)$ was taken to be 1. This was necessary when calculating the maximum potential muscle force during a motion. $f(l)$ was calculated using the normalized length-force relationship curve (Figure 6) and the muscle lengths exported from OpenSim. The activation level can be between 0 and 1. In order to calculate the maximum potential muscle force, it was assumed to be 1, maximum activation.

3.2. Once all of the physiological muscle parameters are determined, how can the muscle forces be determined? Figure 12 shows the free body diagram of the system.

Figure 12: Free body diagram of the system

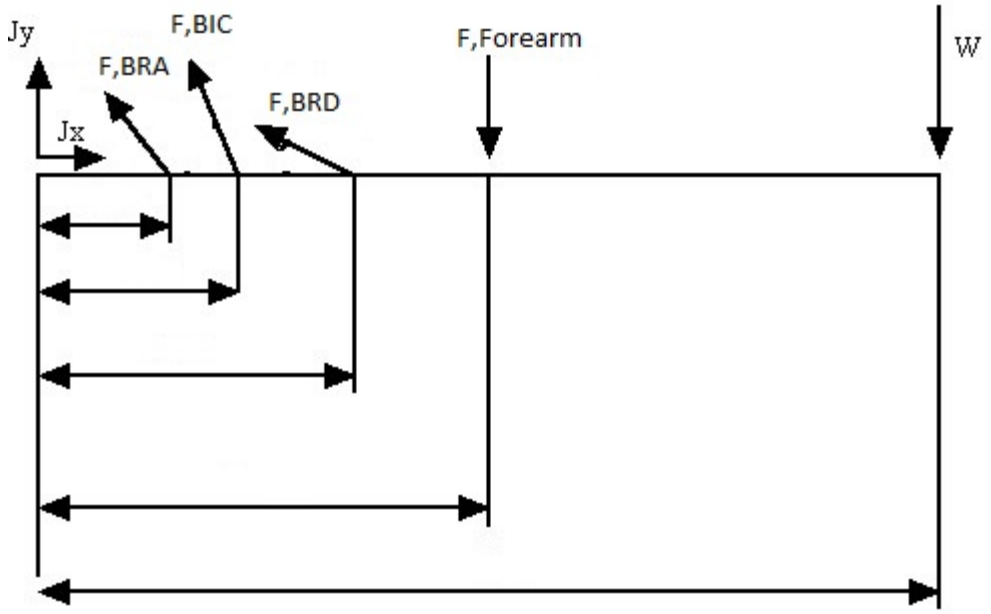

The elbow joint can be modeled as a lever with five forces acting on it. From this diagram we can derive

$$M_{net} = F_{BIC}\, r_{BIC} + F_{BRA}\, r_{BRA} + F_{BRD}\, r_{BRD} + F_{forearm}\, r_{forearm} + F_{resistance}\, r_{resistance}\ . \quad (6)$$

Here M_{net} is the net joint moment, F_{BIC} is the force of the BIC, F_{BRA} is the force of the BRA, and F_{BRD} is the force of the BRD. r_{BIC} is the moment are of the BIC, r_{BRA} is the moment arm of the BRA, and r_{BRD} is the moment are of the BRD. $F_{forearm}$ is the force due to the forearm's weight (1.9 kg as reported by Saul et al. (2014)), $r_{forearm}$ is the forearm's moment arm, $F_{resistance}$ is the force due to the resistance, and $r_{resistance}$ is the resistance's moment arm. The joint contact forces are not modeled because they are

small, and it will only complicate the model. The optimization procedure might not converge to an actual minimum if the joint contact forces are put into the equation (Li et al. 2006). Different joint centers can lead to different solutions, and the absolute true joint center must be known in order for this equation to work. Neglecting joint reaction moments is equivalent to modelling the elbow as a frictionless rotation joint. Furthermore, the antagonist muscles were not modeled because the elbow flexors do the vast majority of the work, and the triceps only becomes active at the very end of the motion. This assumption is supported by several EMG studies (Wilkie 1949, Pauly et al. 1967). Therefore, we have 1 equation with 3 unknowns. There are two ways to solve this indeterminate problem: forward dynamics and inverse dynamics.

3.3. In forward dynamics, a system is setup with muscles (actuators) acting on the skeletal system. The system is then driven by the activation levels as the input. The muscle model is responsible for the transformation of the activation signal to muscle force in order for the model to achieve the desired motion or goal. The joint moment is then the sum of the muscle forces multiplied by their moment arms. Using the joint moment, multijoint dynamics can be used to compute the accelerations, velocities, and angles for the joint during the motion.

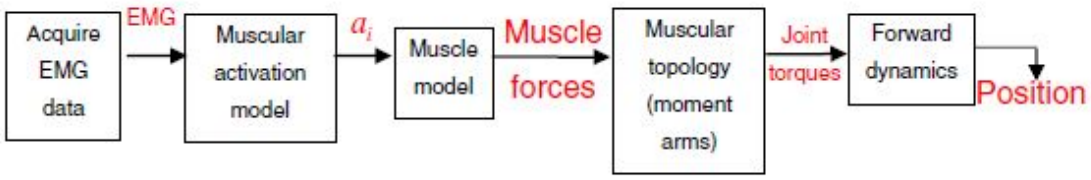

Figure 13: Forward Dynamics method (Pontonnier and Dumont 2009).

There are several problems when using forward dynamics. First, forward dynamics requires either the use of EMG signals taken from the subject during motion or the estimation of the activation levels. EMG signals are very inconsistent, and their transformation to muscle force is difficult (Zajac and Gordon 1989, Buchanan et al. 2004, Pontonnier and Dumont 2009). Small errors in activation levels can lead to drastic errors in the joint position.

3.4. Inverse dynamics begins with measuring the position and external forces using a motion capture system. By tracking markers on a subject, the segment positions, velocities and accelerations can be calculated using inverse kinematics. Next, inverse dynamics is used to calculate the joint moment. From the joint moment, the muscle forces can be estimated using optimization. In order to do this, the inertia and mass of each body segment must be known and has been documented in the work done by Saul et al. (2014). Figure 14 presents the flowchart for the inverse dynamics approach which is used in this study.

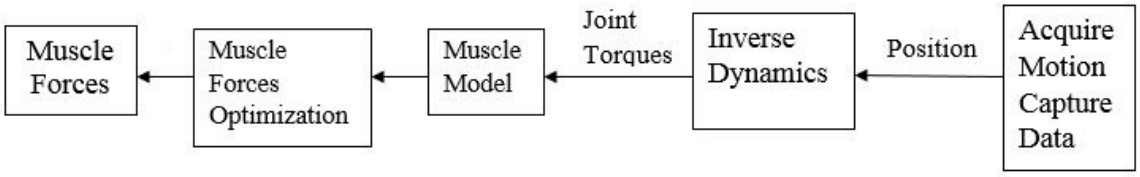

Figure 14: Inverse Dynamics method, modified after Pontonnier and Dumont (2009).

However, inverse dynamics is not without its flaws. Joint moments can be grossly miscalculated when there is co-contraction involved, such as when a subject is walking (Buchanan et al. 2004). However, co-contraction is not a problem in this study because the elbow extensors are minimally activated during a curl. Inverse dynamics is better

suited for determining muscle forces in this situation because it takes into account the speed of elbow flexion. Then, physiological constraints can be put on the muscles during optimization to force them to behave as a muscle should. In order to use inverse dynamics, several pieces of information are needed: the kinematic motion, muscle parameters, and external load. Once the inverse dynamics solution has been calculated, the estimation of the muscle forces can be determined.

CHAPTER 4: METHOD

4.1. There are two common forms of resistance while doing the curl: free weight and strength band. The free weight is a dumbbell that is attached to nothing and is held in the hand while the subject performs the curl motion. It is commonly used by body builders, athletes, and rehabilitation programs. The strength band is an elastic band, of varying tensions, that is attached to a fixed point at one end while the other end is held in the subject's hand. The band is stretched, and the tension increases as the exercise is performed. So, the band has a low resistance at the beginning of the exercise and a high resistance at the end. Strength bands are more popular with rehabilitation trainers, but they are also used by athletes and body builders as well. The end of the strength band is commonly fixed either by stepping on the end of it or by tying it to a stationary point in front of the subject. Figure 15 shows the three different exercises tested.

Figure 15: Three different exercises tested. Left- Free Weight (FW). Middle- Strength band with attachment point at the foot of the subject (SB Foot). Right – Strength Band with attachment point 1 foot in front of the subject (SB Floor).

In order to determine the moment created by either the strength band or the free weight, the moment arm had to be calculated. The free weight's moment arm (as well as the forearm's moment arm) was calculated using

$$r_R = L_F sin(\theta) \ . \tag{7}$$

Here r_R is the free weight's or forearm's moment arm, L_F is the length from the elbow joint center to the center of the hand (or the center of the elbow), and is the joint angle.

4.2. The motion data for this study was taken using a 10 camera 3D Motion Capture System (Vicon, Oxford, UK) at 60 Hz. This motion capture system tracks the displacements of reflective markers that are placed on the subject. The subject wore a tight, sleeveless shirt and the markers were taped directly onto the skin. The same marker placement was used as that of Saul et al. (2014) with some modifications. The markers on the mid-humerus and mid-forearm were not used. These are not anatomical locations, and

their movement due to the flexion of muscles can affect the motion data. The marker placement can be seen in Figure 16.

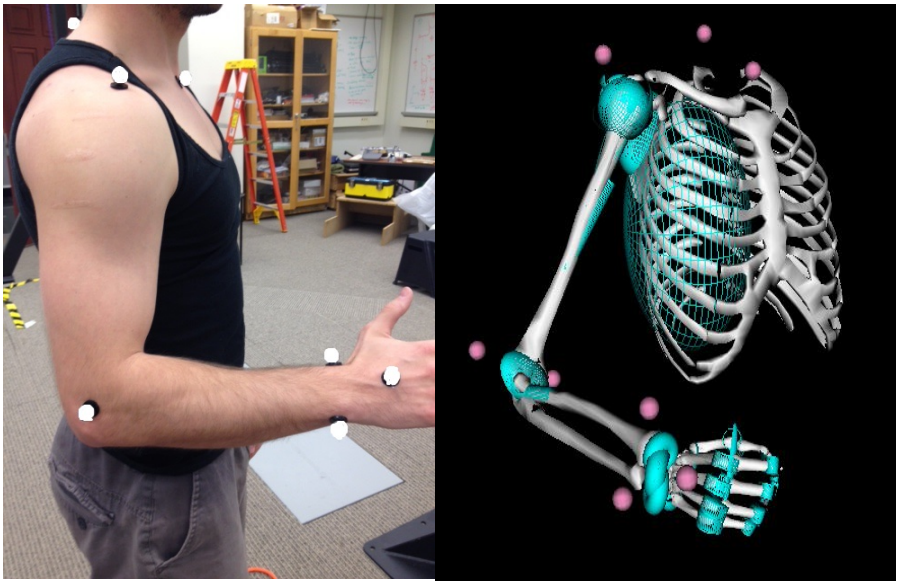

Figure 16: Marker Placement

This marker setup follows the guidelines discussed by OpenSim's support page as well as by Capozzo et al. (1995) in order to accurately capture the motion. The .c3d files that are exported from Vicon must be converted into the proper format that OpenSim can read (.trc). This was done using the MATLAB-OpenSim Interfaces created by Glen Lichtwark, and can be downloaded at simtk.org.

The center of the hand was calculated from the motion capture data using a customized MATLAB code. A marker was placed on both ends of the dumbbell, and Equation 8 was used to calculate the center of the hand.

$$\vec{P} = \left(\frac{x_2 - x_1}{2}, \frac{y_2 - y_1}{2}, \frac{z_2 - z_1}{2}\right) \quad (8)$$

While using the strength band, the band's line of action, length, and moment arm were calculated along with the hand center location. The end of the strength band was fixed

onto a small, light bar that was held in the subject's hand in order to make it easier to grip. A marker was placed on both ends of the bar in order to calculate the center of the hand using Equation 8. A marker was also placed next to the spot where the band was fixed at the other end. From these two positions, the band's length, line of action, and moment arm were calculated.

$$L_{SB} = \sqrt{(x_2 - x_1)^2 + (y_2 - y_1)^2 + (z_2 - z_1)^2} \tag{9}$$

$$\vec{O} = \vec{Q} + t\vec{P} \tag{10}$$

$$\vec{r} = \vec{O} - \vec{S} \tag{11}$$

$$r_{resistance} = \|\vec{r}\| \tag{12}$$

Here L_{SB} is the length of the strength band, $\vec{O}$ is the line of action of the strength band, $\vec{Q}$ is the coordinates of the marker placed at the strength band's attachment point on the ground, $\vec{P}$ is the hand center. $\vec{S}$ is the coordinates of the elbow center using Equation 8, $\vec{r}$ is the coordinates of the point on $\vec{O}$ where, and $r_{resistance}$ is the moment arm of the strength band.

4.3.1. Musculoskeletal simulations are used to analyze the roles of muscles during movements. OpenSim is a freely available, user extensible software system that lets users develop models of musculoskeletal structures and create dynamic simulations of movement. OpenSim has emerged as a powerful tool to uncover the mechanics of movement, and it is an important reference in the biomechanical world. OpenSim was developed by Delp et al. (2007) to study the dynamics of individuals with pathological gait and to explore the biomechanical effects of treatments. Today, it has evolved into user-programmable software to create and explore biomechanical models. The software

provides a platform for the biomechanics community to build a library of muscle and skeletal models. Models have been developed that simulate movement of the lower and upper extremities according to clinical data found in research. They can be used to test, analyze, modify, and improve biomechanical simulation of human movement. The models are freely accessible to everyone allowing constant addition and modification of any biomechanical and physiological characteristics of the skeletal or muscular systems that the user wishes to research or analyze.

4.3.2. The model used in this study was developed by Saul et al. (2014). It is a dynamic model that represents the 50th percentile adult male and can be downloaded at simtk.org. The kinematic foundation for this model was created by Holzbaur et al. (2005). It has 15 degrees of freedom at the glenohumeral joint, elbow, forearm, wrist, thumb, and index finger with 50 Hill-type muscle-tendon actuators representing the 32 muscles and muscle compartments crossing the shoulder, elbow, forearm, and wrist. The kinematic version of this model has also been used by Pontonnier and Dumont (2009). Saul et al. (2014) added all of the body segments' (bones) inertial properties to the kinematic model.

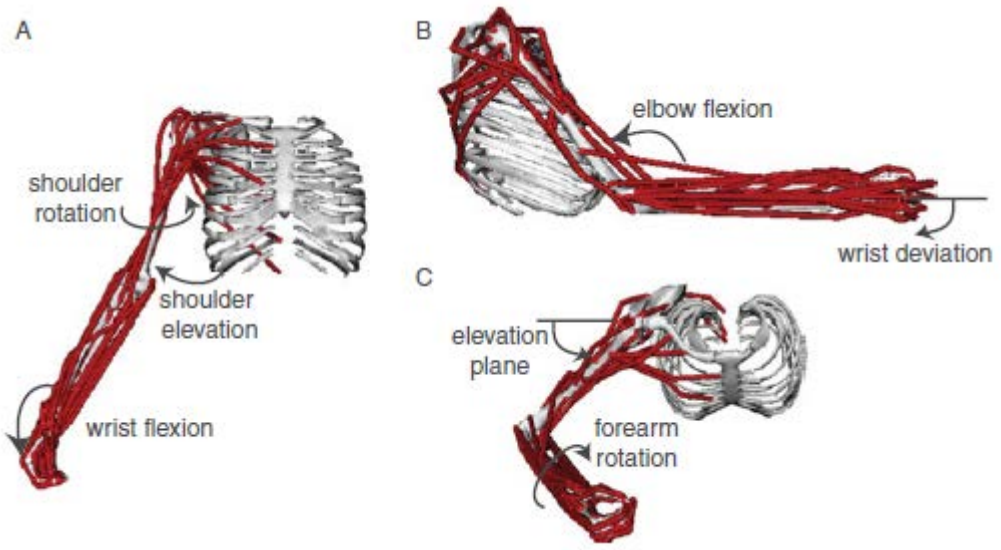

Figure 17: Musculoskeletal model of the upper limb. The dynamic model has 7 degrees of freedom and 50 muscle actuators, (Saul et al. 2014).

4.4 Once the motion data had been captured, OpenSim was used to scale and compute the inverse kinematics solution. The scaling process in OpenSim scales the mass properties and the dimension properties of the body segments. In measurement-based scaling, scale factors are determined by comparing distances between markers on the model and experimental marker positions provided by the motion capture data. OpenSim uses a weighted least squares equation to solve for the general coordinates of the body segments.

$$\min_{q}\left[\sum_{i=\#\ of markers} w_i \left|x_i^{exp} - x_i(q)\right|^2 + \sum_{\substack{j=unprescribed \\ coord}} w_j (q_j^{exp} - q_j)^2\right] \quad (13)$$

Here q is the vector of generalized coordinates being solves for, x_i^{exp} is the position of the marker recorded by Vicon, and x_i^q is the position of the marker on the model. w_i and w_j are marker and coordinate weights which can be specified in OpenSim in order to

track some markers with greater accuracy than others. No markers were weighted in this study. This least squares problem is solved using a general quadratic programming solver, with a convergence criterion of 0.0001 and a limit of 1000 iterations. Total RMS and maximum marker errors are reported by OpenSim. The maximum marker error should be less than 2-4 cm, and the RMS should be under 2 cm. The model was scaled and inverse kinematics calculated following these guidelines.

Once the kinematic motion had been imported to OpenSim, there were several key muscle parameters that could be exported: muscle moment arm, normalized muscle fiber length, muscle fiber length, and joint angle. The muscle moment arm was calculated by OpenSim. OpenSim tracks the line of action of each muscle during the motion and automatically computes that muscle's moment arm with respect to the joint it crosses. The normalized muscle fiber length curve was also exported using OpenSim. The model has a set optimal fiber length that can be adjusted, and the normalized fiber length is recorded during the motion. This curve was used to calculate the muscle's maximum force potential using the normalized length-force curve.

4.5. In order to simulate resistance in the model's hand, an external force file (.mot) had to be created with the force point locations and vectors. The dumbbell has a static weight creating a force only in the y-direction. Figure 18 shows the coordinate system in OpenSim. So, the creation of the force file for it was easy.

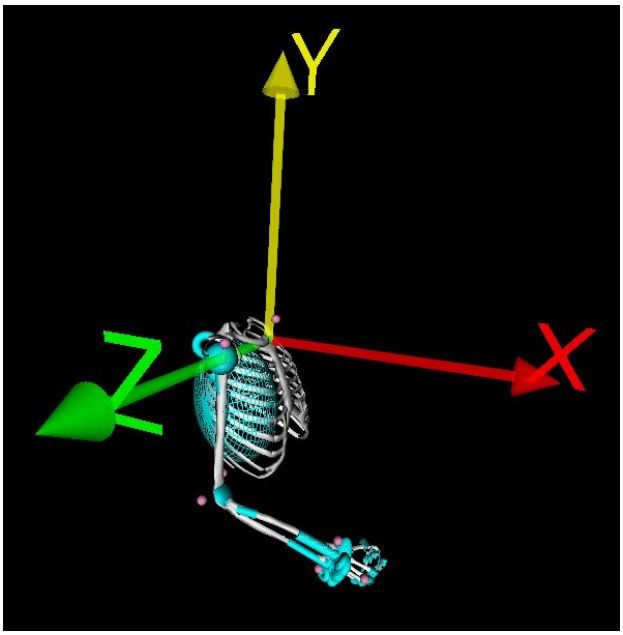

Figure 18: OpenSim coordinate system.

In order to calculate the force vector for the strength band, the magnitude of the tension in the band had to be computed first. Length-tension measurements were taken for light and heavy tension strength bands. The lengths of the bands were chosen so that their tension would be 0 N when the elbow joint angle was at 0°. Next, the bands were hung from the metal frame in the motion lab. The length of the band was measured while weights of 0, 2.5, 5, 7.5, 15.5, and 22.5 pounds were hung from the bottom of the band. The setup is shown in Figure 19, and the results can be seen in Table 4.

Figure 19: Length-tension experimental setup.

Table 4: Length-tension results.

	0 [lb]	2.5 [lb]	5 [lb]	7.5 [lb]	15 [lb]	17.5 [lb]	22.5 [lb]
Strength Band Length (Light) [m]	0.7	0.74	0.83	0.98	1.57	-	-
Strength Band Length (Heavy) [m]	0.70	0.71	0.765	0.815	1.00	1.17	1.40

From this data, the magnitude of the tension in the band during the motion could be estimated by using Hooke's Law and calculating the length of the band from the motion capture data. Using the coordinates of Q and P, the force vector for the strength band can be calculated using Equations 14-16.

$$F_{SB,x} = F_{SB}\left(\frac{P_x - Q_x}{L_{SB}}\right) \quad (14)$$

$$F_{SB,y} = F_{SB}\left(\frac{P_y - Q_y}{L_{SB}}\right) \quad (15)$$

$$F_{SB,z} = F_{SB}\left(\frac{P_z - Q_z}{L_{SB}}\right) \quad (16)$$

Here Q is the coordinates of the marker that is fixed at the strength band's origin, F_{SB} is the magnitude of the tension in the band, L_{SB} is the length of the strength band, and $F_{SB,xyz}$ is the force vector in the x,y,z directions. Once the force vectors were calculated, the external force file was created using Tim's Gait Extraction Toolbox.

4.6. Inverse dynamics is a method for computing moments of forces based on kinematic motion of a body and its inertial mass properties. The body segments' inertial mass properties are reported by Saul et al. (2014). OpenSim has a built in tool to determine the net torques at each joint responsible for a given motion by using Newton's Second Law. The classical equations of motion can be written in the following form:

$$M(q)\ddot{q} + C(q,q)^{\cdot} + G(q) = T_{net} \quad (17)$$

$$q, \dot{q}, \ddot{q} \bigcup R^N \quad (18)$$

$$M(q) \bigcup R^{N\times N} \quad (19)$$

$$C(q,\dot{q}) \bigcup R^N \quad (20)$$

$$G(q) \bigcup R^N \quad (21)$$

$$T_{net} \bigcup R^N \quad (22)$$

Here $q, \dot{q}, \ddot{q}$ are the vectors of generalized positions, velocities, and accelerations, $M(q)$is the system's mass matrix, $C(q, \dot{q})$ is the vector of Coriolis and centrifugal forces, $G(q)$ is the vector of gravitational forces, and T_{net} is the unknown vector of generalized forces.

4.7. Static Optimization is an extension of inverse dynamics that solves for the muscle forces at every point in time using the net joint moment. Using the Vicon Motion Capture System, the marker positions were recorded at 60 Hz, and through inverse dynamics, the net joint moment was found for every position recorded. Static optimization was used to solve for the muscle forces at every point in time recorded. It works by minimizing a pre-selected objective function subject to constraints. The general form of an optimization problem can be seen in Equation 23.

$$\min_{x} f(x) \; such \; that \begin{cases} A \cdot x \leq b \\ Aeq \cdot x = beq \\ lb \leq x \leq ub \end{cases} \tag{23}$$

Here $f(x)$ is the objective function to be minimized, and x is the solution vector of muscle forces. lb and ub are the lower bound and upper bound of the solution set vector. lb is set to be 1 N and ub is set to be the maximum potential force of each muscle at any given joint angle. A and b are set to enforce the RFG and stress constraints. A is a matrix of coefficients being either each of the muscle's moment arm at that point in time or $\frac{1}{CSA}$ of the muscle at that point in time. b is a column vector of maximum allowable stresses of each muscle and the maximum allowable change in muscle force of each muscle. Aeq and beq are set to enforce the equality constraint (Equation 6). A custom MATLAB code was written using the fmincon function with an interior-point solving algorithm. fmincon attempts to find a constrained minimum of a scalar function with several variables starting at an initial estimate. fmincon was run for every point in time, and the initial estimate was reset to be

the solution that was found. This ensured that the next time the algorithm ran, it would not start at <0,0,0>. Instead it starts at the solution of the previous point in time. This is an important concept because muscles behave according to their previous state.

4.8. Two objective functions were examined relating to the stress and normalized force of the muscle, these were

$$f(x) = \sum_{n=1}^{NM} \sigma_n^N \tag{24}$$

$$f(x) = \sum_{n=1}^{NM} \left(\frac{F_n}{F_{n,max}} \right)^N \tag{25}$$

NM is the number of muscles, N is the exponent of the objective function, □ is the stress of the muscle, $F_{n,max}$ is the maximum potential force of that muscle at that point in time, and F_n are the muscle forces to be found. N was set to 2 for all of the trials as suggested by Challis and Kerwin (1993). Increasing N does not have a large effect on the muscle force results (Raikova 1996). It is necessary to minimize both Equation 24 and 25. Equation 24 represents a theory in Darwinism that humans naturally perform motions in a way that reduces stress (injury) in the muscles. For example, when the BIC has too much stress on it, it is at risk for injury. The brain will then activate the BRA and BRD to take stress off the BIC. Equation 25 represents another theory in Darwinism that humans use their strongest muscles to do more work than the weaker ones. For example, the BRA will generate a higher force than the BRD because it is stronger. Equations 24 and 25 are very common to use in static optimization. Equation 24 has been used by Kaufman et al. (1991), An et al. (1984), Challis (1997), Crowninshield (1978), Challis and Kerwin (1993), and many other studies as the objective function. Equation 25 has been used by

Challis (1997), Challis and Kerwin (1993), Pontonnier and Dumont (2009), and Herzog (1987) as the objective function.

4.9. Any individual muscle must have a force greater than zero and less than the maximum potential force (An et al. 1989). The upper and lower bounds of the solver were calculated at every point in time using the normalized fiber length data exported from OpenSim. Using the normalized length-force curve, the normalized fiber length was used to calculate $f(l)$ in Equation 5. By solving Equation 5, the upper bound was set so that the muscle's force could not exceed F_m. The lower bound was set to be 1 N. Muscles are limited by how much force they can generate, as well as, how fast they can generate it. The rate of force generation can be found by taking the derivative of the maximum torque curve of each muscle (Andersen and Aagaard 2006), (Aagaard et al. 2002). After the maximum potential force was calculated, the torque of each muscle was calculated with respect to the joint angle using Equation 1. Next, the curve was fit with a quintic polynomial. The maximum change in torque between points in time could then be set using Equation 26.

$$\frac{\mathrm{T}_2 - \mathrm{T}_1}{\Theta_2 - \Theta_1} \leq RTG_{max} \tag{26}$$

Here T_2 is the maximum torque that the muscle can generate at the current point in time, T_1 is the maximum torque that the muscle could generate at the previous point in time, $\Theta_{1,2}$ are the corresponding joint angles, and RTG_{max} is the maximum allowable increase in torque. The limit was also set for the maximum stress that each muscle could withstand to be 100 $N \cdot \ cm^{-2}$, (An et al. 1989). An equality constraint was put on the solver. The

sum of all of the forces times their moment arms had to be equal to the net joint moment exported by OpenSim. Equation 6 shows the equality constraint.

4.10.1. First, the Vicon Motion Capture System was calibrated, and all background markings that the system might pick up were either taped over or masked using the Vicon software. Next, a template was made of the marker setup. The subject wore a tight, black sleeveless shirt, and the markers were taped onto the anatomical positions in Figure 16. The subject was then told to perform the different exercises using a comfortable, controlled motion while maintaining joint angular velocity. The subject was also told to start with the elbow as close to 0° of flexion as was comfortable with forearm supination. Overall, three trials were recorded. The first was done with the subject holding a 15 lb dumbbell, Figure 15-Left**.** The second trial was done while the heavy strength band was attached at the foot, Figure 15-Middle. The third trial was done while the heavy strength band was attached 1 foot in front of the subject, Figure 15-Right.

After the motion capture data had been recorded, the marker positions were imported into OpenSim, and scaling and inverse kinematics were done. Next, the external load files were created. For Trials 2 (SB Foot) and 3 (SB Floor), two different external load files were created. One was for the light strength band, and the other was for the heavy strength band. Next, the loads were imposed on the model using inverse dynamics. After the inverse dynamics solution had been calculated, joint moment, muscle moment arms, normalized muscle lengths, muscle lengths, and the joint angle were exported into a customized MATLAB script. Table 5 shows all of the different combinations of exercises, resistances, and objective functions analyzed.

Table 5: Objective functions and forms of resistance tested.

	Min Norm Force	Min Stress	External Load	Attachment point
Trial 1 (FW)	✓	✓	Free Weight	-
Trial 2 (SB Foot)	✓	✓	Strength Band: Light and Heavy	Foot
Trial 3 (SB Floor)	✓	✓	Strength Band: Light and Heavy	1 ft. in front of subject

The MATLAB script was written to perform static optimization using physiological muscle constraints. The length-force relationship and maximum potential force (Equation 5), joint moment equality (Equation 6), rate of force generation (Equation 26), stress constraints (Equation 2), and objective functions (Equations 24 and 25) were put on the optimizer in order to calculate the muscle forces according to physiological properties. The MATLAB script was run, calculating the minimal muscle force, according to its physiological parameters, to achieve the net joint moment for every point in time. Figure 19 shows the basic method used for this study. The method for this study is related to the steps taken by Pontonnier and Dumont (2009).

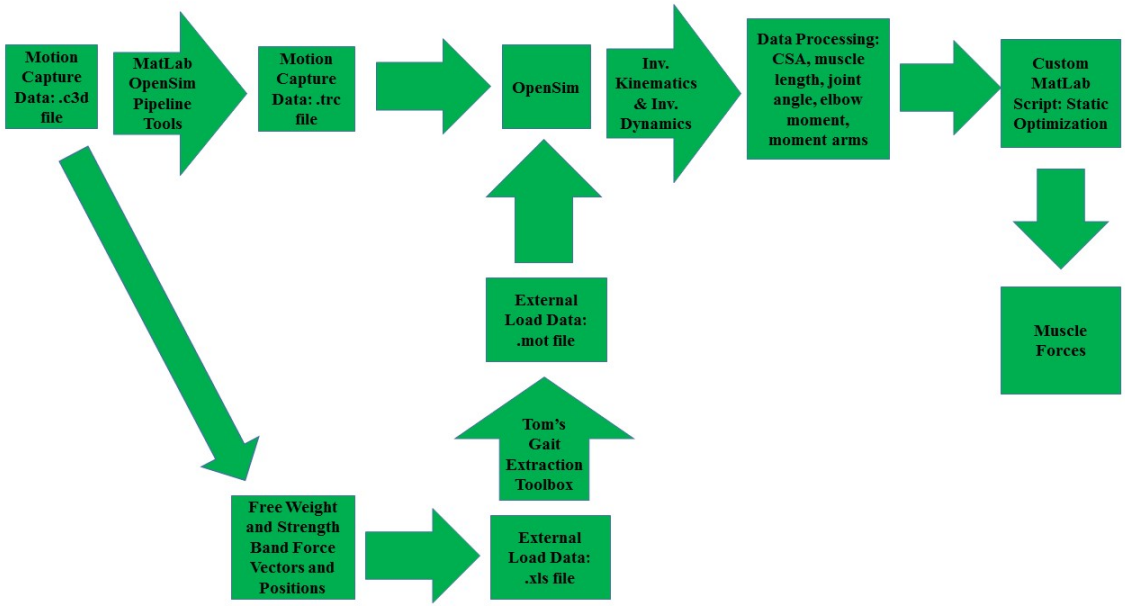

Figure 19: Basic setup used in this study.

4.10.2 In addition to the muscle force calculation, the effects of shoulder and forearm rotation on the maximum muscle force were examined. The markers were placed on the subject in the same anatomical locations as discussed in Chapter 4.2**.** Next, the motion capture system was calibrated, and the subject was told to perform the curl motion without an external resistance. Once the motion capture data had been recorded it was imported into OpenSim. OpenSim has the ability to restrict any joint from rotating. By locking a joint, it restricts that joint from moving during the imported motion without changing the motion of other joints. Selected joints were locked in place in order to examine the effects that different shoulder and forearm angles had on where the maximum of the muscle force curve would occur. All joint angles were set to a predetermined value and locked in that position except for the elbow which has a range of motion from 0 to 130 . To investigate the effects that forearm rotation has on the

elbow flexors, the forearm was locked in three different positions during the kinematic motion: 90° (Pronation), 0° (Neutral), and -90° (Supination).

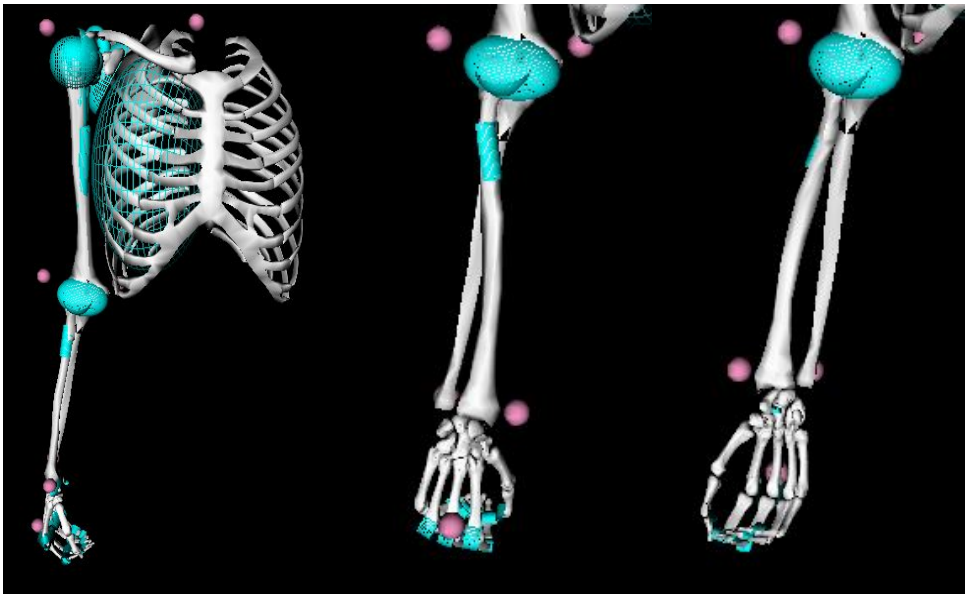

Figure 20: Left- forearm (neutral) with all other joints locked. Middle- -90° (Pronation) thumb pointing toward body. Right- 90° (Supination) thumb pointing away from body.

Shoulder flexion and rotation were locked at 0° (arm down at the side). To investigate the effects of shoulder elevation, the shoulder was locked at two different angles: 0° and 90°. The difference between the two can be seen in Figure 21. The forearm was locked at 0° of rotation (neutral). The BIC is the only muscle that crosses the shoulder. So, maximum forces were not calculated for the BRA and BRD because shoulder movement has no effect on them.

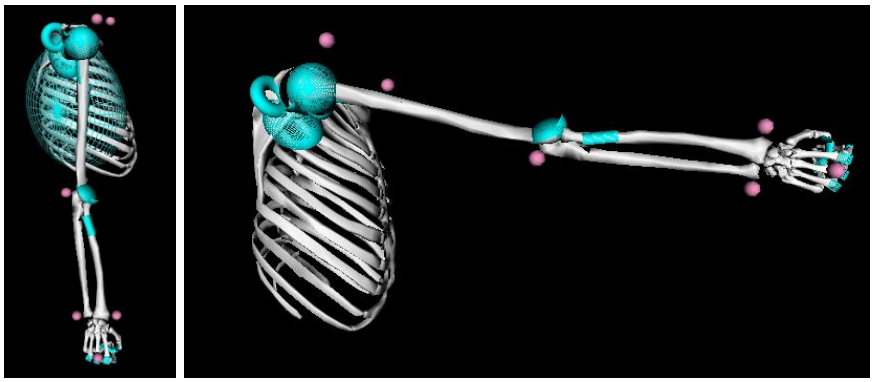

Figure 21: Left- shoulder elevation at 0° Right- shoulder elevation at 90°

To investigate the effects of shoulder rotation, the shoulder's rotational angle was set at two different angles: 25° and -45°. The difference can be seen in Figure 22. The forearm was locked at 0°.

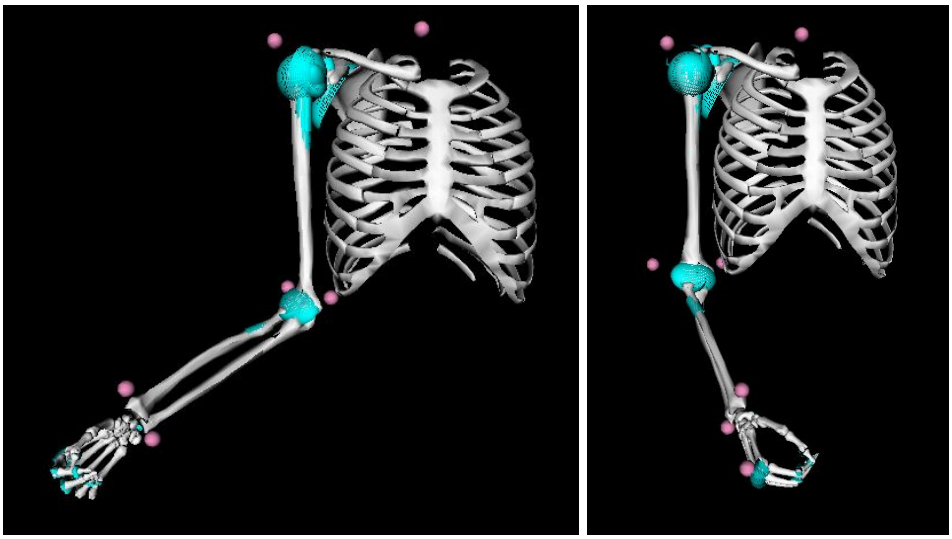

Figure 22: Left- shoulder rotation at -45° Right- shoulder rotation at 20°

The normalized muscle lengths were exported through OpenSim for all trials, and the maximum muscle force was calculated using the normalized force length curve and Equation 5. The results of this trial are very beneficial to trainers who want to know how different forms of the curl can affect the way the elbow flexors are being worked.

CHAPTER 5: RESULTS

5.1.

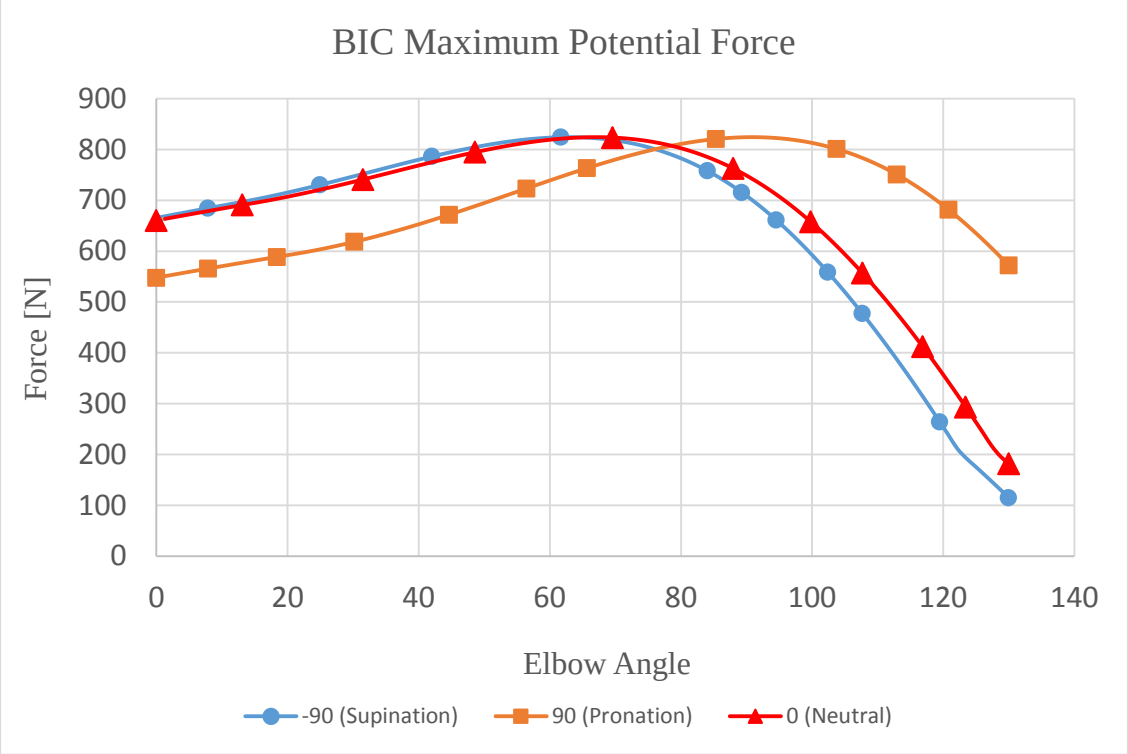

Figure 23: Forearm Supination/Pronation effect on the BIC maximum potential force during a curl.

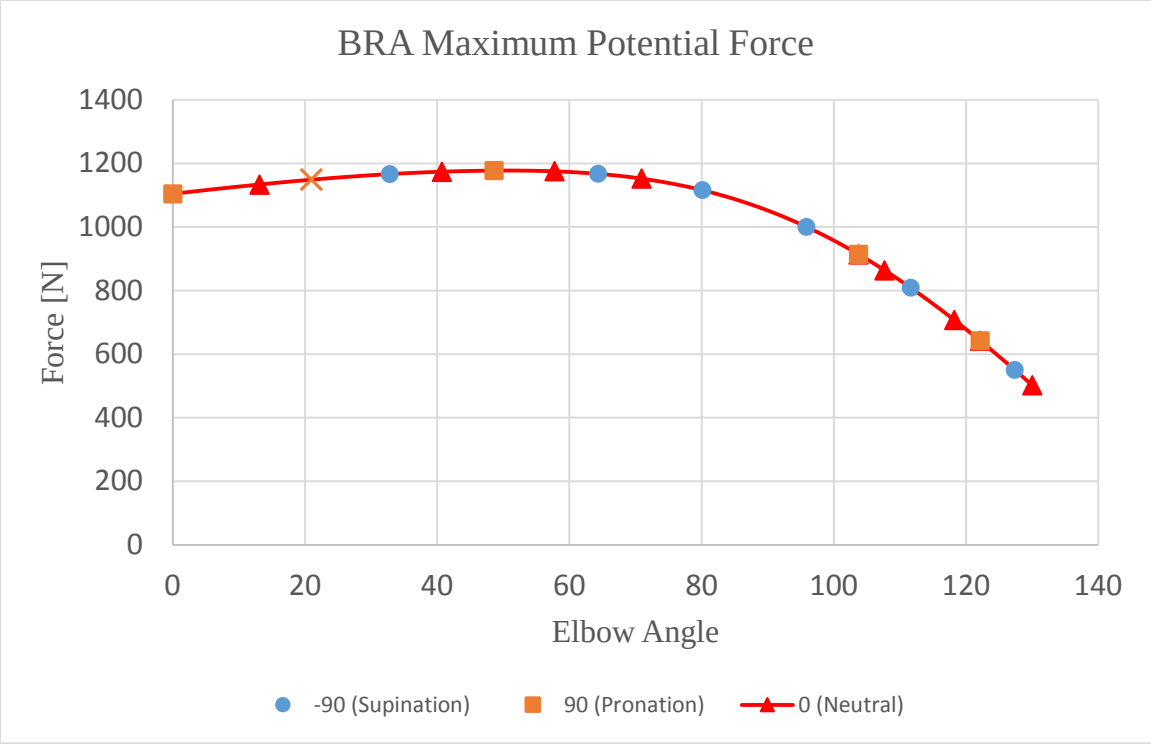

Figure 24: Forearm Supination/Pronation effect on the BRA maximum potential force during a curl.

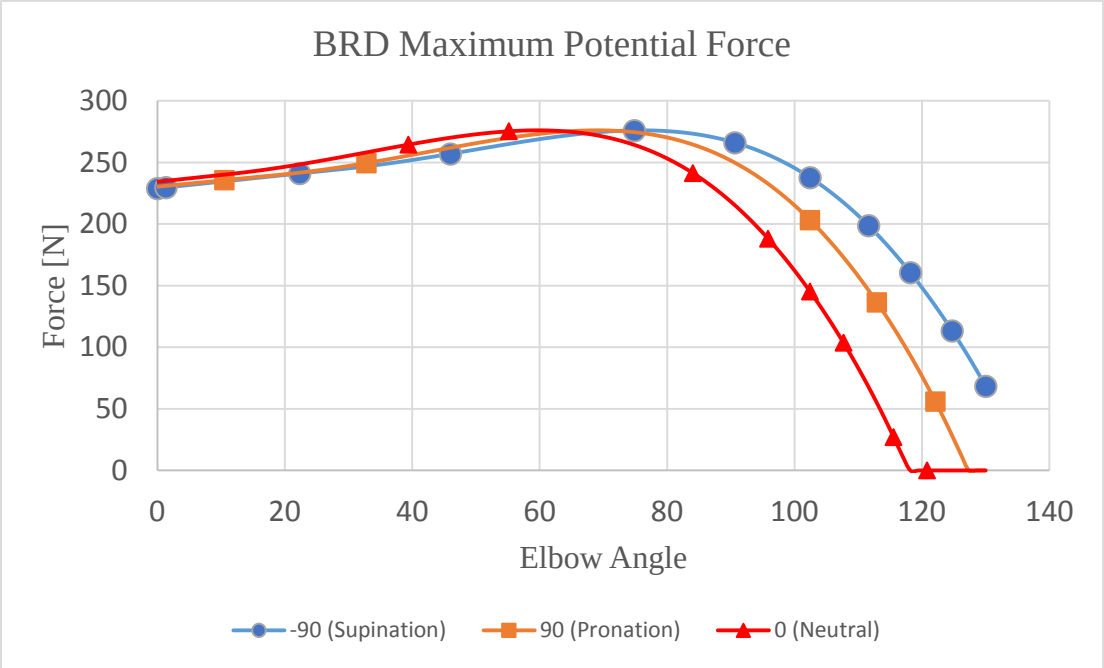

Figure 25: Forearm Supination/Pronation effect on the BRD maximum potential force during a curl.

The effects of forearm pronation/supination on the elbow flexors can be seen in Figures 23-25. It should be noted that markers on all of the plots do not represent the only data points that were recorded. They are only there to help distinguish between the different curves. Forearm pronation/supination had a large effect on the maximum potential force that the BIC could produce. The BIC is partially responsible for the pronation/supination of the forearm. Contraction of the bicep can be observed easily by simply rotating one's forearm. At pronation the BIC is at a long length, and at supination it is at a shorter length. It should be no surprise that, going from pronation to supination will progressively cause the maximum muscle force peak to occur earlier in the curl motion. Pronation/supination had a very minimal to no effect on the BRA. The BRA attaches to the ulna, but it is so close to the elbow joint center that rotation of the forearm has almost no effect on it.

Forearm rotation had a significant effect on the BRD. The BRD is attached to the outside of the radius, crosses over the top of the forearm, and attaches to the outside of the humerus. Naturally, the BRD plays a big role in the rotation of the forearm. The BRD is at its shortest length (when comparing supination/pronation/neutral positions) when the forearm is in the neutral position. Therefore, the peak of the maximum potential force curve will occur earlier in curl motion.

The results of shoulder elevation can be seen in Figure 26. Figure 26 shows that elevating the arm (flexion of the shoulder muscles) shortens the BIC slightly. The BIC's maximum potential force will occur earlier in the motion with a shoulder elevation angle of 90□.

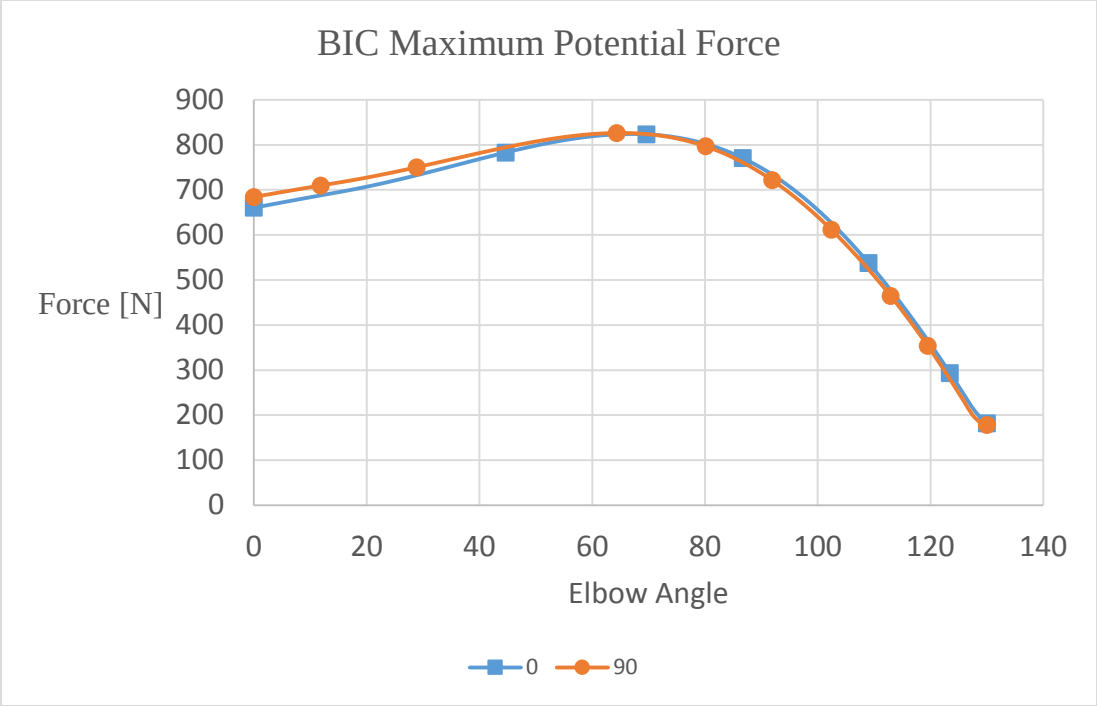

Figure 26: Shoulder elevation effect on the BIC maximum potential force during a curl.

The effects of shoulder rotation can be seen in Figure 27. Figure 27 shows that shoulder rotation has an effect on the BIC maximum potential force curve. By rotating the shoulder inward, the BIC is shortened. Therefore, its maximum potential force will occur earlier during the curl motion.

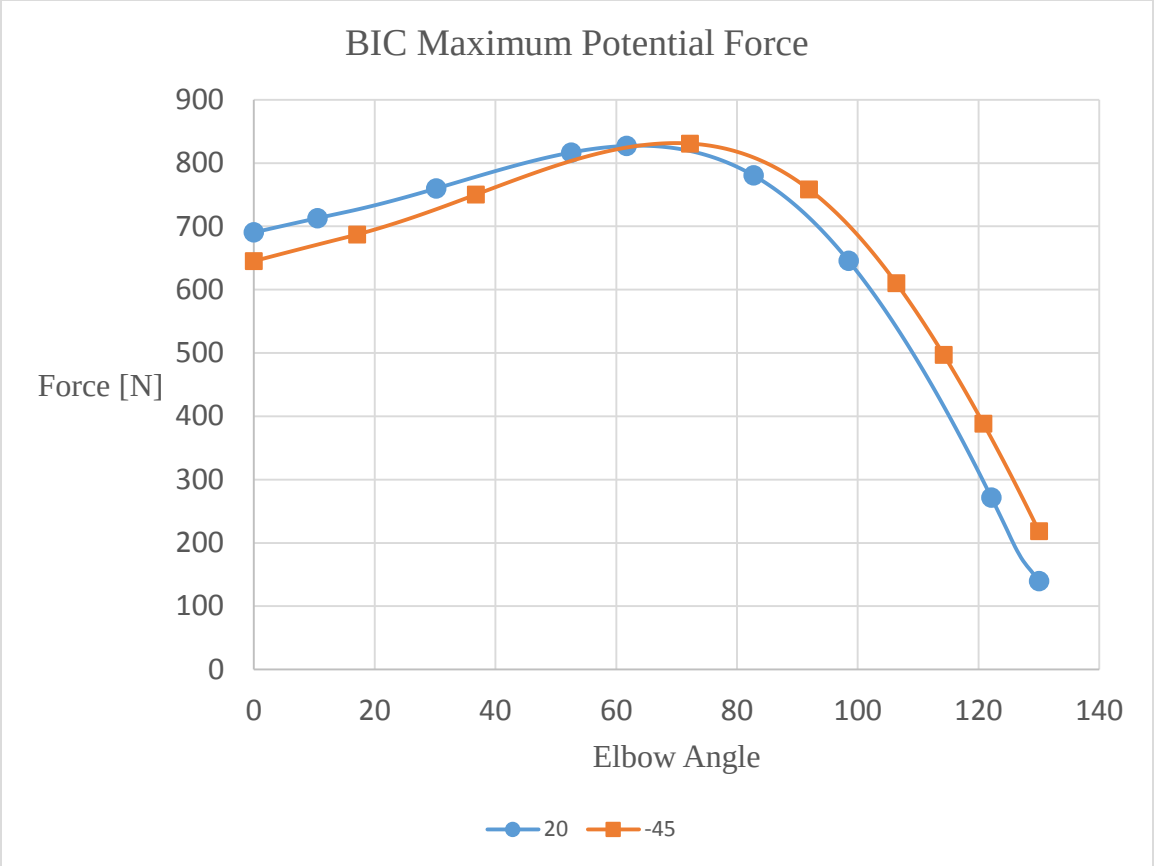

Figure 27: Shoulder rotation effect on the BIC maximum potential force during a curl.

5.2. For the data analysis, the moment arms of the BIC, BRA, BRD, and resistance were recorded for each trial. The moment arms for the BIC and BRA were consistently the same for all of the trials. It should be noted that the kinematic motion in Trial 3 (SB Floor) started at 18□ of elbow flexion. Due to higher forces in the x-direction from the strength band, the elbow flexors were already partially contracted in order for the subject to start the motion with their hand at the side. In other words, the band was pulling the arm forward, and in order for the subject to keep the hand at their side the elbow flexors had to be activated. Also, the kinematic motions of Trial 1 (FW) and 2 (SB Foot) were very similar when compared to each other while the resistance in Trial 3 (SB Floor) caused a slightly different motion. Some key characteristics in the three motions can be seen in Table 6.

Table 6: Key kinematic characteristics of the 3 exercises.

	Average Supination Angle	Starting Elbow Angle	Average Shoulder Rotation Angle
Trial 1	70.30	0	4.68
Trial 2	71.51	0	5.50
Trial 3	59.14	18	3.69

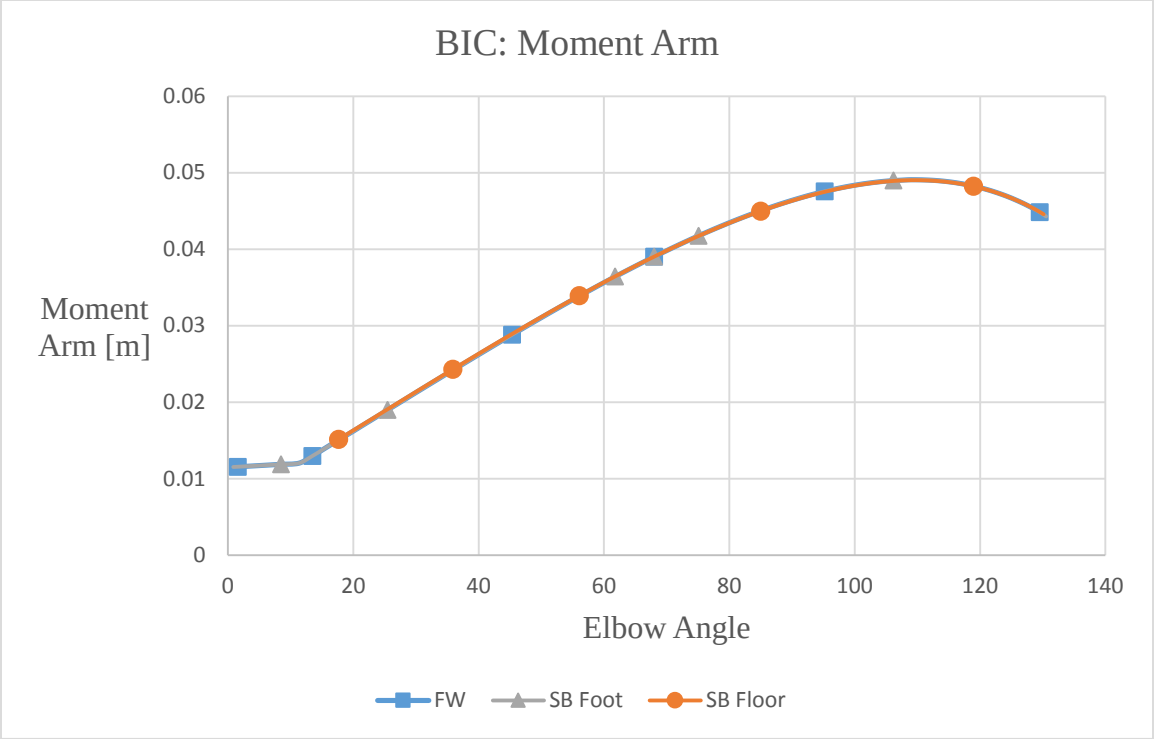

Figure 28: Comparison of the BIC moment arm between the three trials.

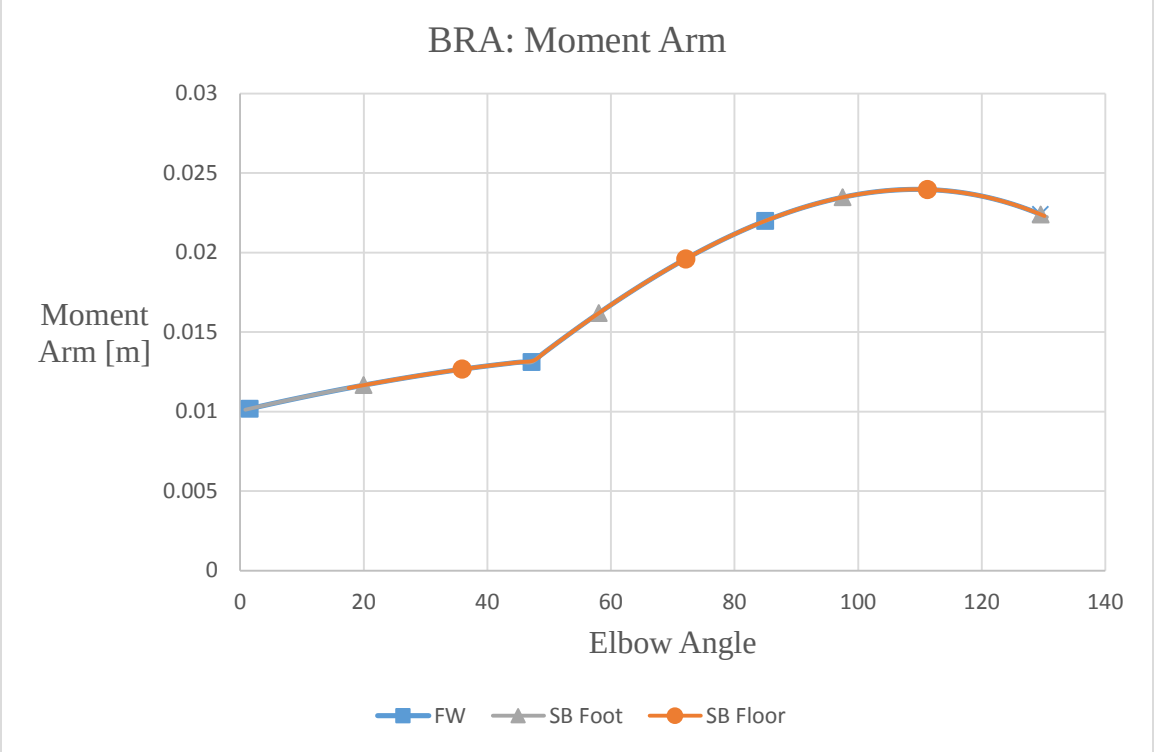

Figure 29: Comparison of the BRA moment arm between the three trials.

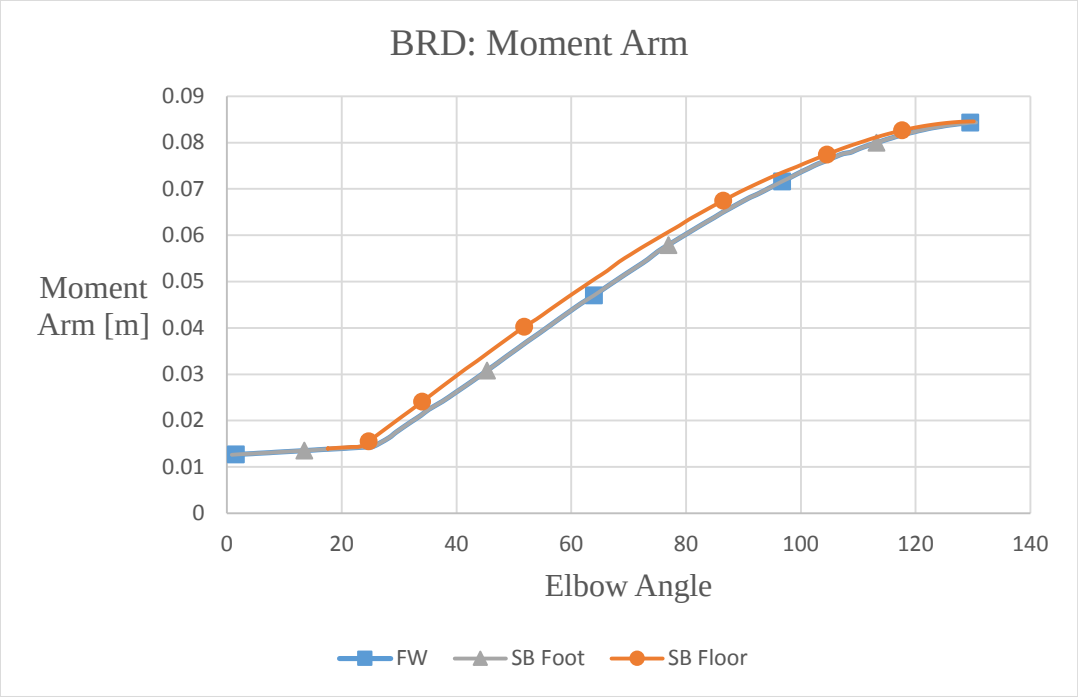

Figure 30: Comparison of the BRD moment arm between the three trials. The BRD has a peak moment at 130° of elbow flexion.

The BIC has a peak moment arm at an elbow angle of 109° of elbow flexion. The moment arm of the BIC steadily increases from elbow angles of 0° to 109°. Then, it starts to decrease as the attachment point on the forearm starts to come back towards the elbow joint center. The attachment point can be thought of as travelling around the joint center in an arc. At 109° of elbow flexion, the attachment point is at its furthest point from the elbow joint center. At other points along the arc, the attachment point is closer to the elbow joint center, thus, moving the BIC's line of action closer to the elbow joint center.

The BRA has a peak moment arm at an elbow angle of 109°. From elbow angles of 0° to 48°, the BRA attachment point is very close to the center of the elbow, and the BRA tendon lies almost on top of the joint as can be seen in Figure 1. At 49° of flexion, the moment arm begins increasing at a faster rate due to the BRA's attachment point on

the ulna moving away from the elbow center. The BRA's moment arm had a minimal change between the three exercises.

The only muscle to show a difference in the moment arm between the three trials was the BRD. In Trial 3 (SB Floor), the subject had an average supination angle of 54.7°. In Trials 1 (FW) and 2 (SB Foot), the average supination angle was 73.3° and 70.6°. This had minimal effect on the BIC and BRA, but 18.6° less of supination lifted the BRD attachment point on the radius slightly above the elbow joint center in the y-direction, thus increasing its moment arm slightly.

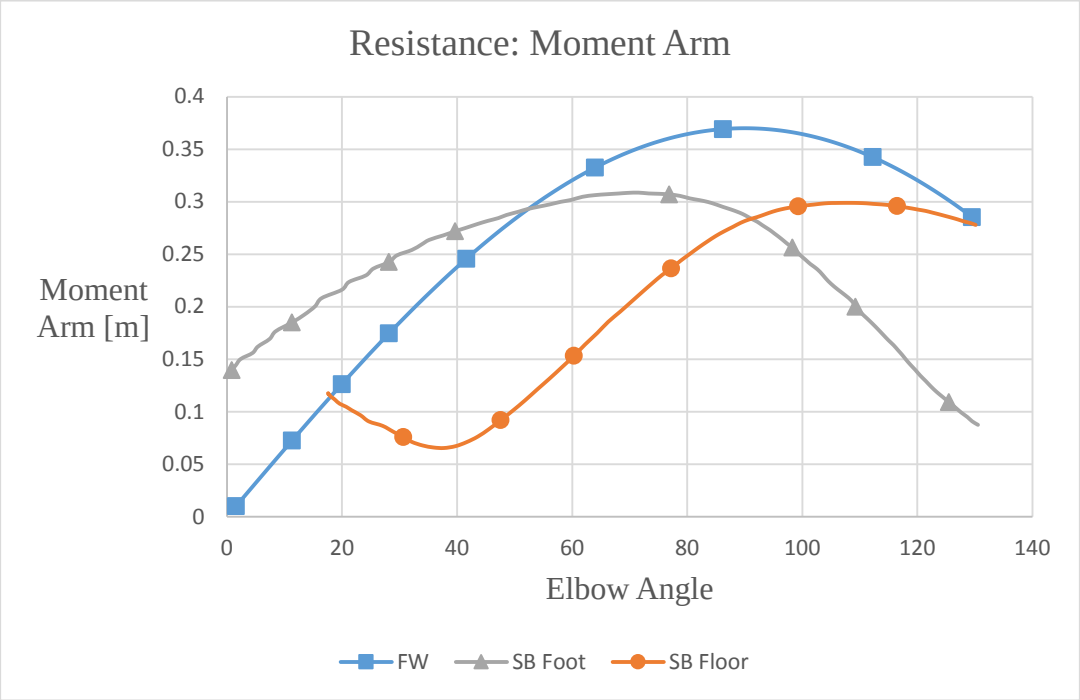

Figure 31: Comparison of the resistance moment arms between the three trials.

There was a significant difference in the resistances' moment arms. The strength band in Trial 2 (SB Foot) had the largest moment arm from elbow angles 0° to 51° of flexion. After 51°, the free weight had the largest moment arm. Moving the strength band's attachment point forward Trial 3 (SB Floor) had a critical effect on the band's

moment arm. The strength band's line of action almost passes directly through the elbow center at 38□of flexion. Then, the moment arm increases to be higher than Trial 2 (SB Foot) at an elbow angle of 92□. The resistance's moment arm will become crucial when evaluating the moment of resistance.

The normalized muscle lengths were recorded in order to determine where the maximum potential force for each muscle would occur during the kinematic motions. The normalized muscle lengths are reported in Figures 31-34.

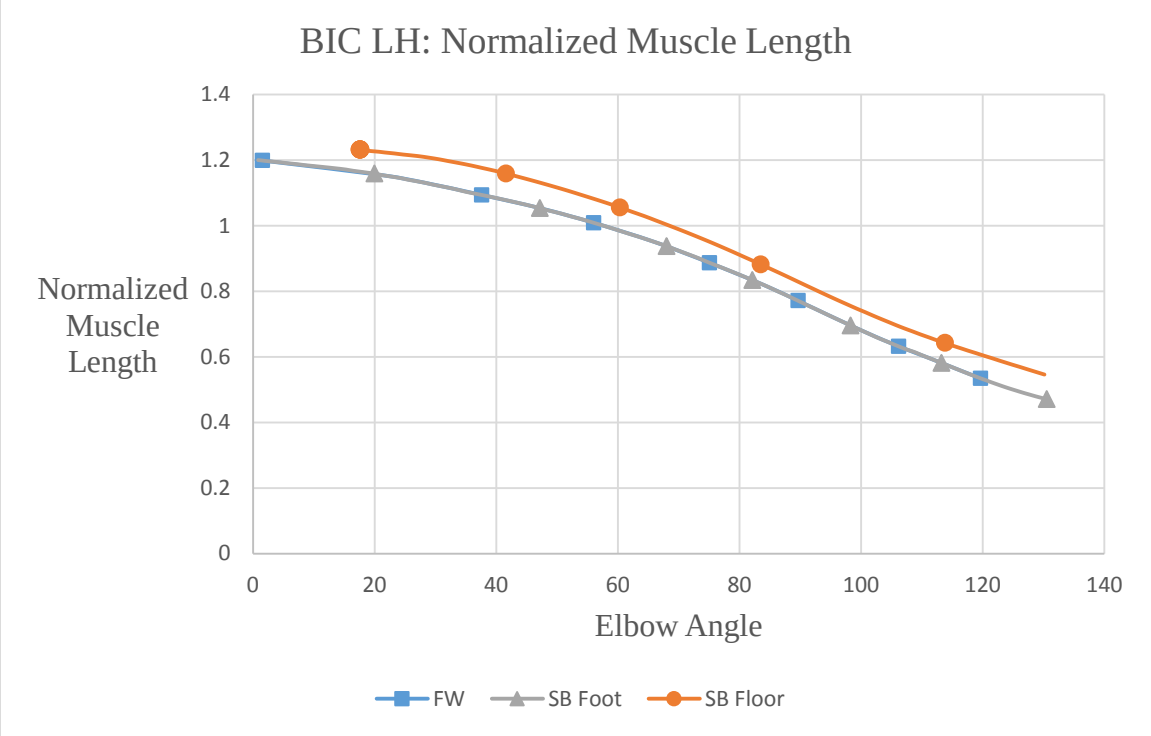

Figure 31: Comparison of the normalized muscle length curves between trials for the BIC LH.

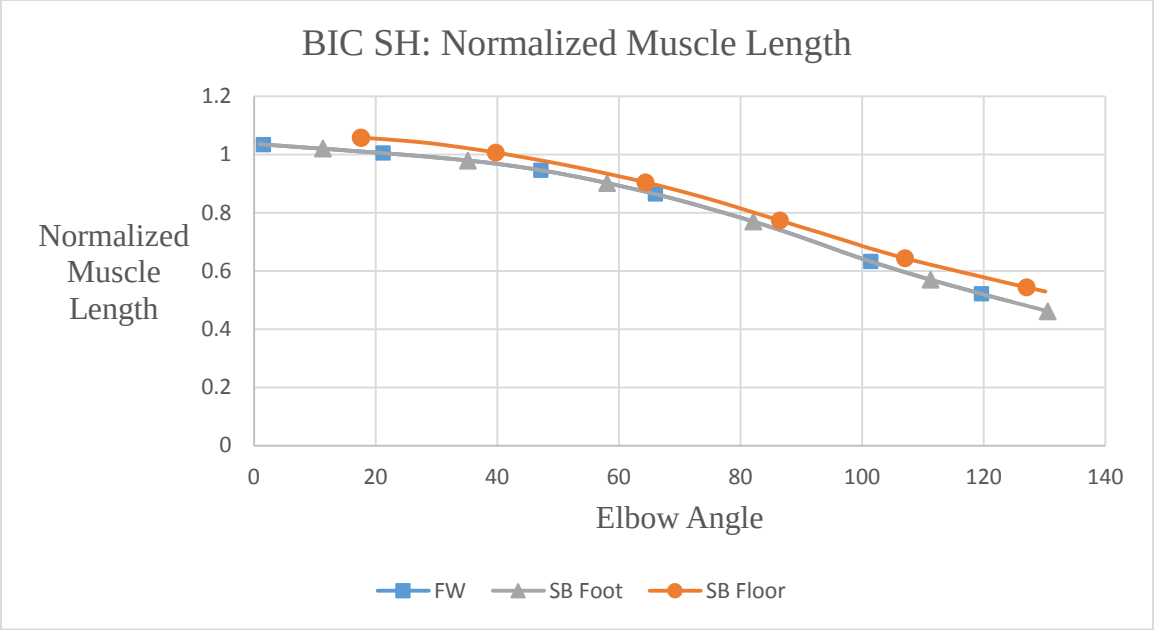

Figure 32: Comparison of the BIC SH normalized muscle length curves between trials for the BIC SH.

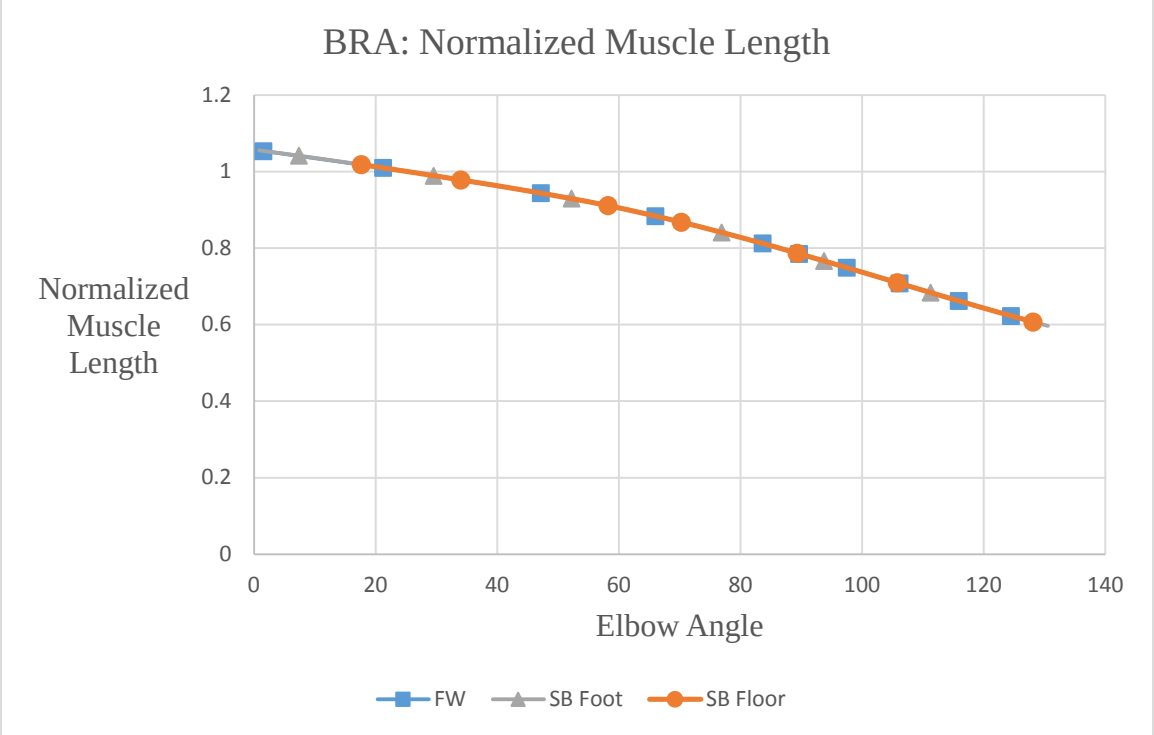

Figure 33: Comparison of the normalized muscle length curves between the different trials for the BRA.

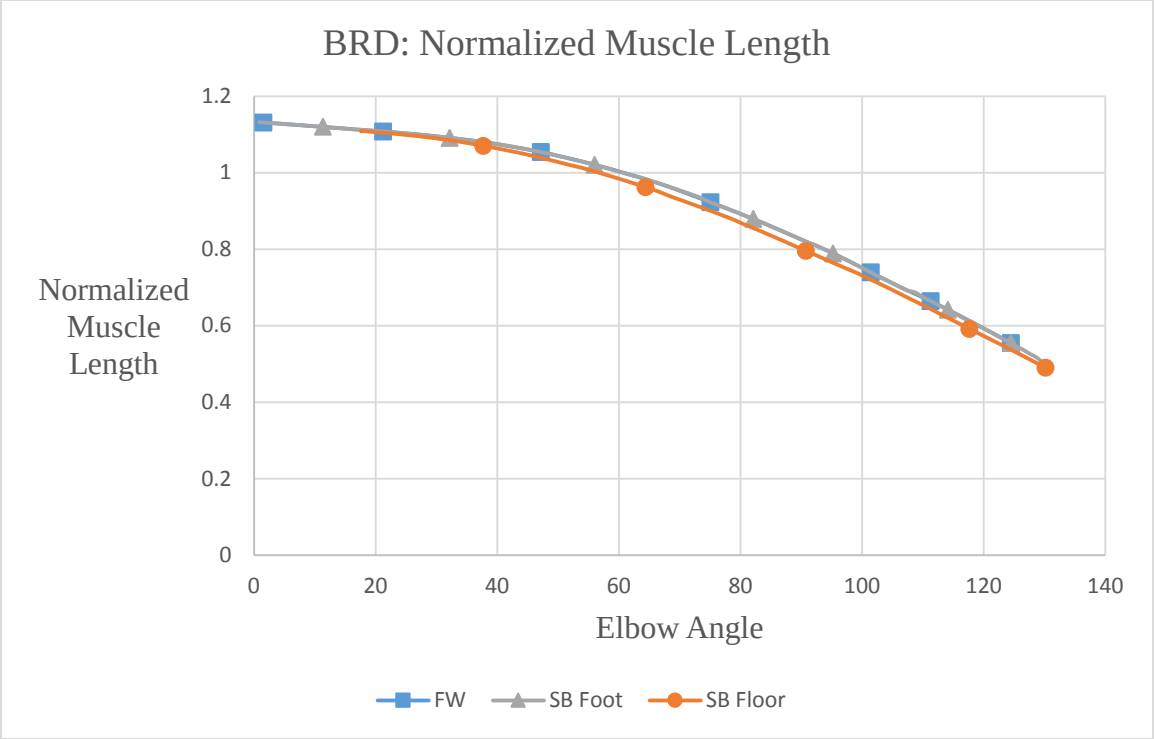

Figure 34: Comparison of the normalized muscle length curve between different trials for the BRD.

No significant differences were found between Trial 1 (FW) and Trial 2 (SB Foot). The normalized muscle length curves behave as expected. The elbow flexors contract steadily throughout the curl motion. During Trial 3 (SB Floor), the subject had less supination than in Trials 1 (FW) and 2 (SB Foot). This explains why the BIC LH and BIC SH are longer at given joint angles and why the BRD is shorter at given joint angles when compared to Trials 1 (FW) and 2 (SB Foot).

The maximum torque curve for each muscle was computed at each point in time using Equation 1. The results of the Trials 1 (FW), 2 (SB Foot), and 3 (SB Floor) can be seen in Figures 35-37. The maximum torque curve is important because it determines the rate of force generation and the maximum moment that the muscles can sustain at any point in time.

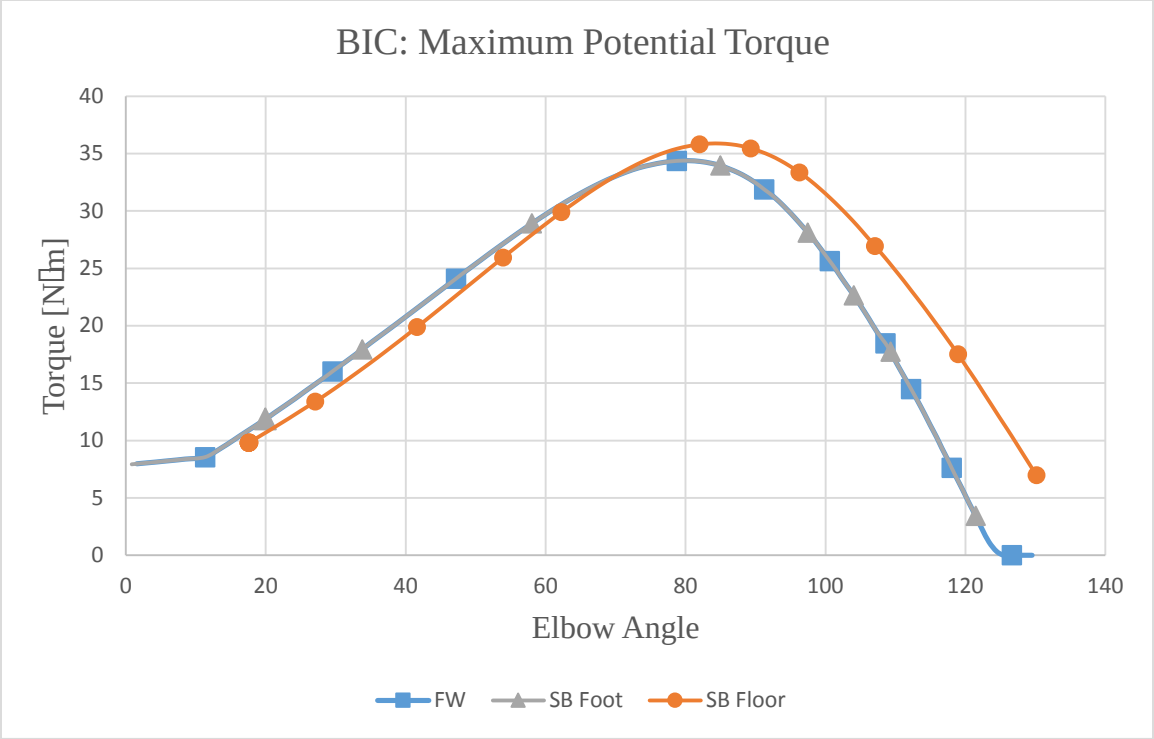

Figure 35: Comparison of the maximum potential torque that can be generated by the BIC during the three trials.

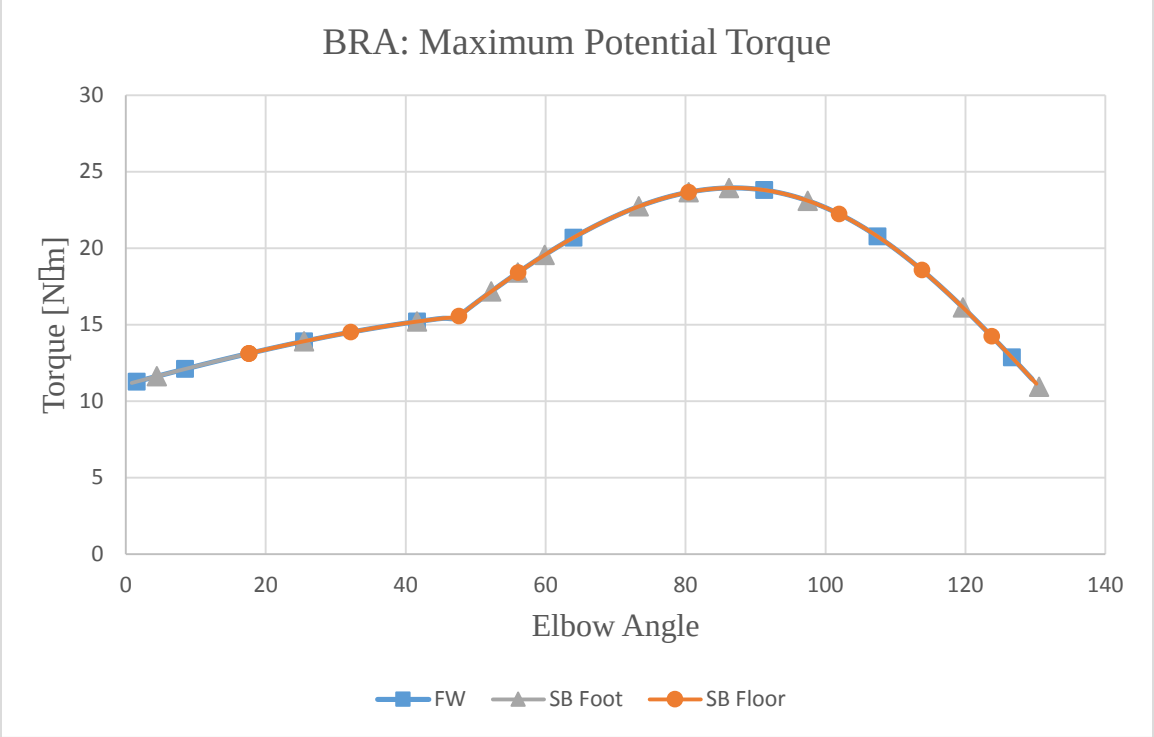

Figure 36: Comparison of the maximum potential torque that can be generated by the BRA during the three trials.

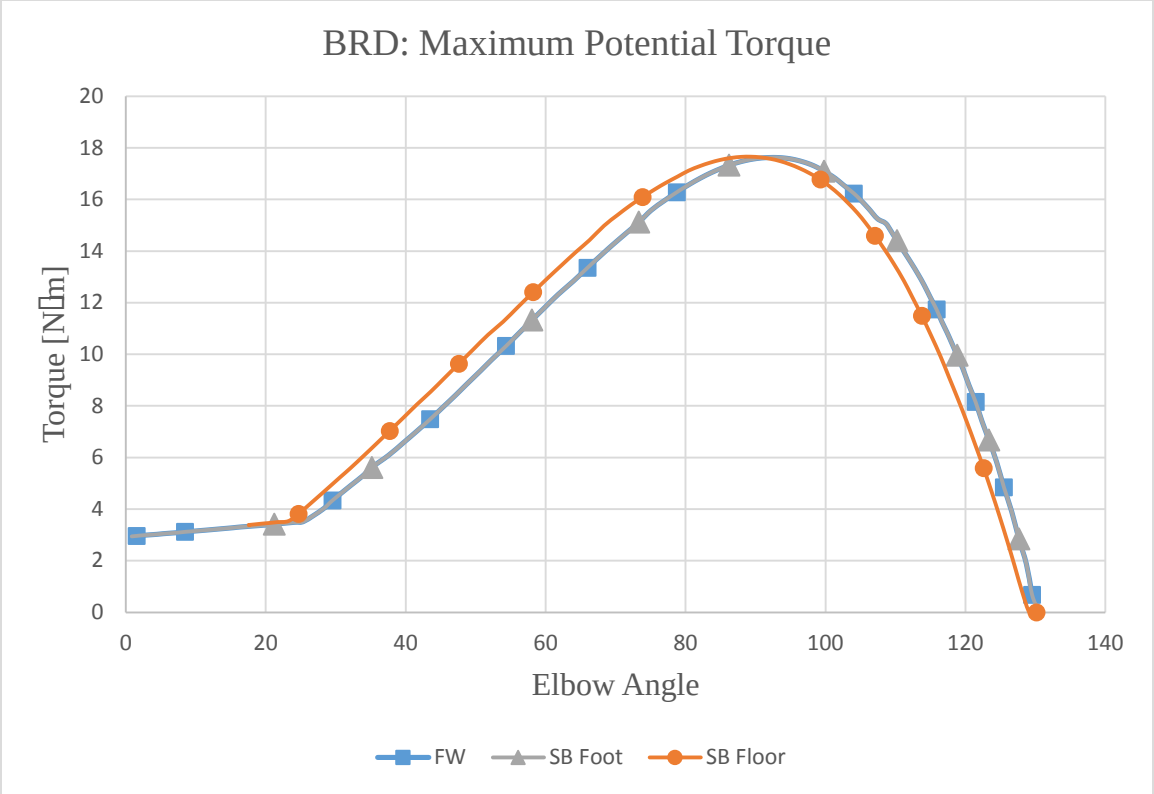

Figure 37: Comparison of the maximum potential torque that can be generated by the BRD during the three trials.

The BIC has a peak potential torque at an elbow angle of 80□ for Trials 1 (FW) and 2 (SB Foot), and 86.5□ for Trial 3 (SB Floor). The peak is also greater in Trial 3 (SB Floor) at 35.8 $N \bullet m$ compared to Trials 1 (FW) and 2 (SB Foot) at 34.4 $N \bullet m$. Due to the smaller supination angle during Trial 3 (SB Floor), the peak of the maximum potential muscle force occurred later in the motion. However, Figure 28 shows that the moment arm of the BIC did not change significantly between Trials 1 (FW), 2 (SB Foot), and 3 (SB Floor). So, this leads to less potential torque in Trial 3 (SB Floor) at elbow angles of 0□ to 70.3□, and more potential torque from 70.3□ to 130□. The opposite can be said about the BRD. The BRD maximum torque curve's peak occurs at 90.7□ (17.6 $N \bullet m$) and 94.9□ (17.4 $N \bullet m$) of elbow flexion. A smaller supination angle in Trial 3 (SB Floor) lead to shorter

muscle lengths, resulting in the maximum potential force occurring earlier in the motion. From 23.2° of elbow flexion to 90.7° of elbow flexion, there is greater potential torque, and less potential torque from 90.7° to 130°. There was no significant change in the BRA maximum potential torque because it is minimally affected by forearm supination/pronation.

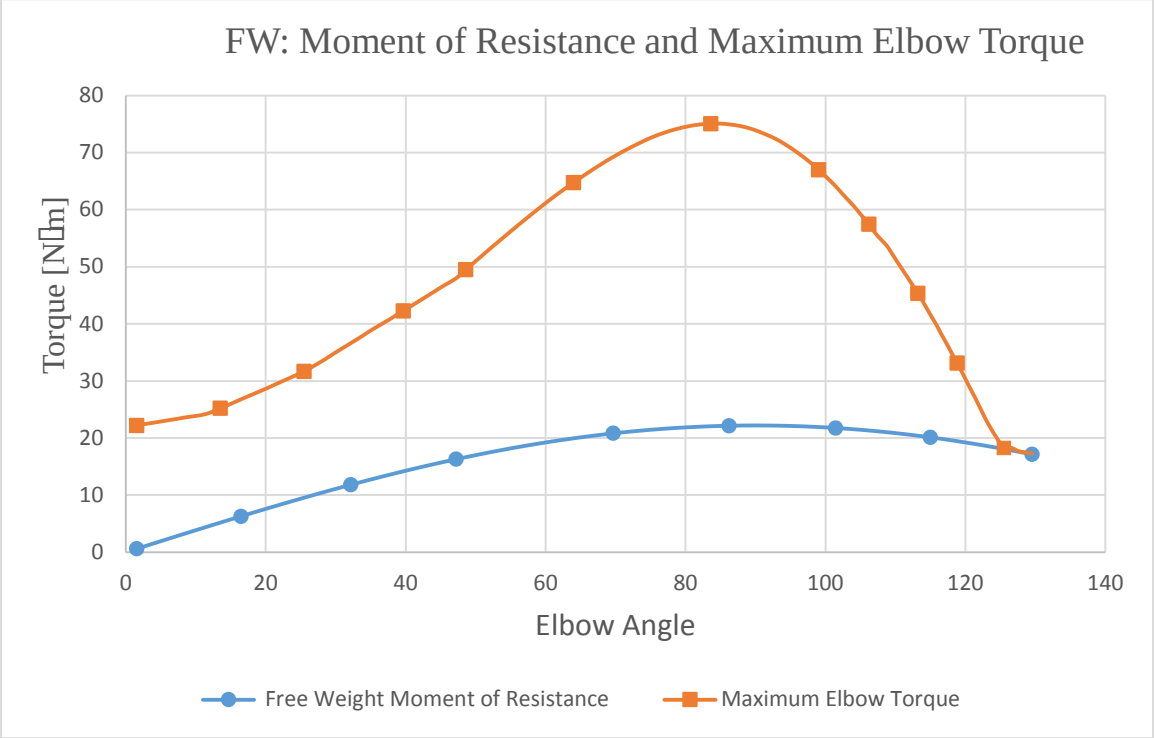

Figure 38: Comparison of the moment of resistance created by the free weight and the maximum torque that can be generated by the elbow flexors for Trial 1 (FW).

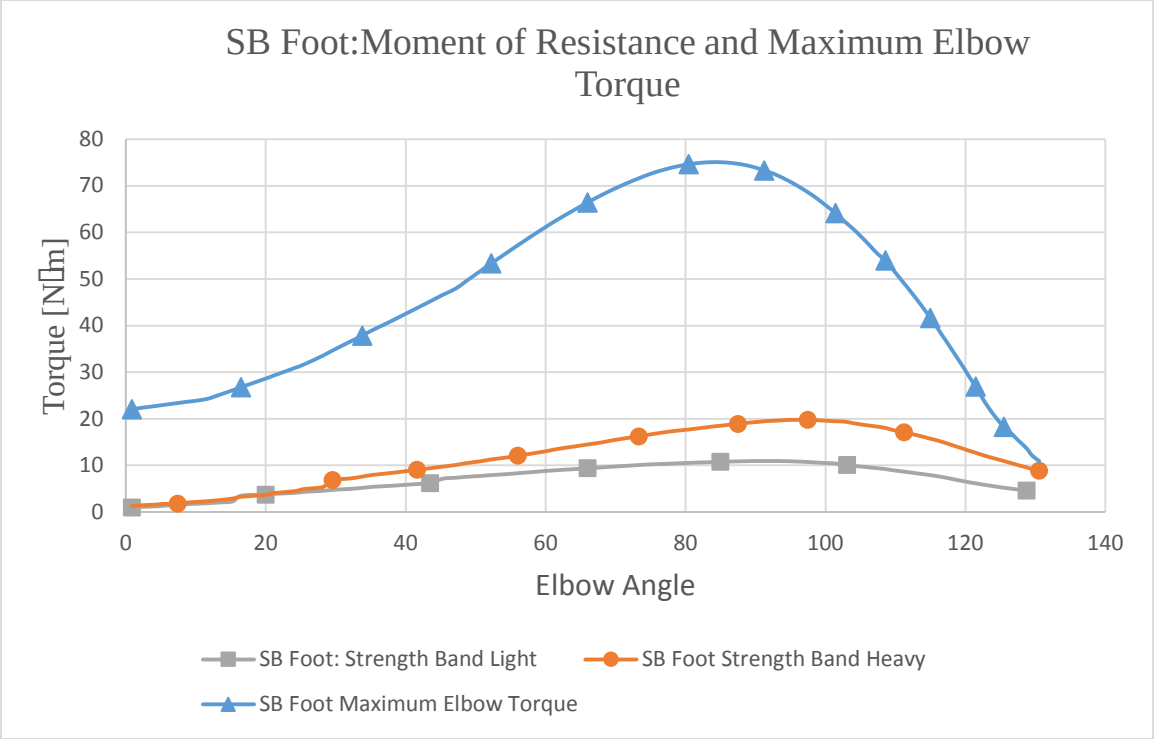

Figure 39: Comparison of the moment of resistance created by the strength bands and the maximum torque that can be generated by the elbow flexors for Trial 3 (SB Floor).

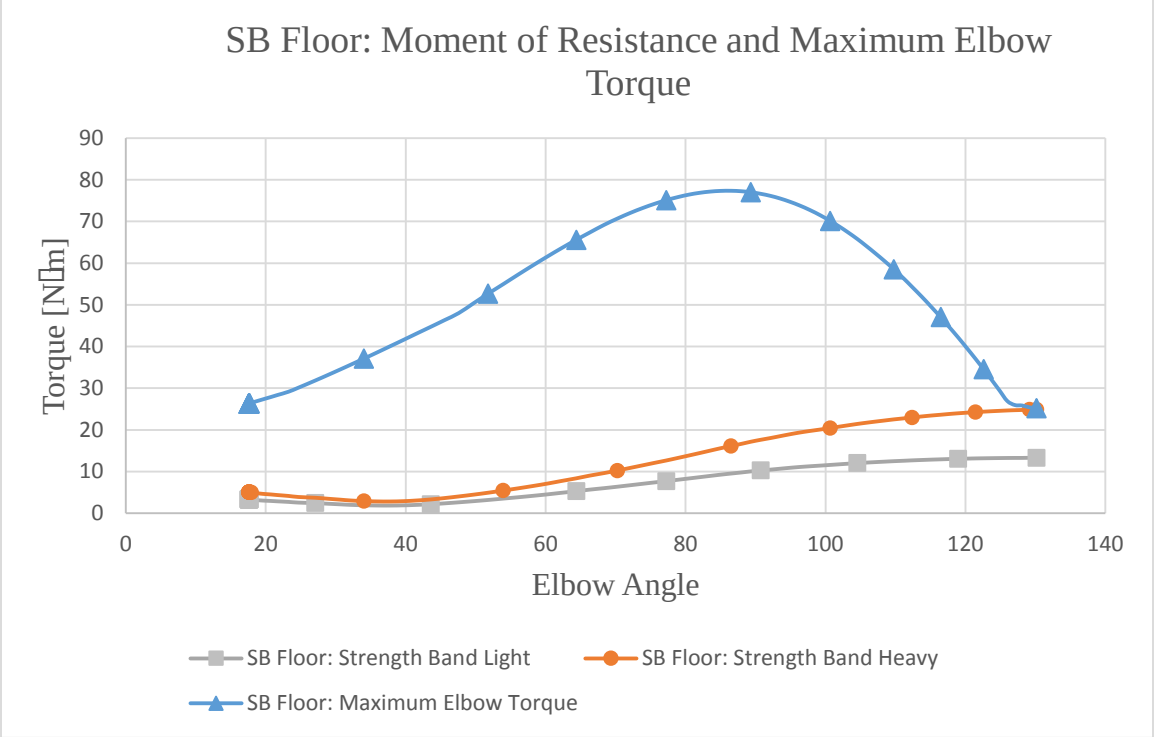

Figure 40: Comparison of the moment of resistance created by the strength bands and the maximum torque that can be generated by the elbow flexors for Trial 3 (SB Floor).

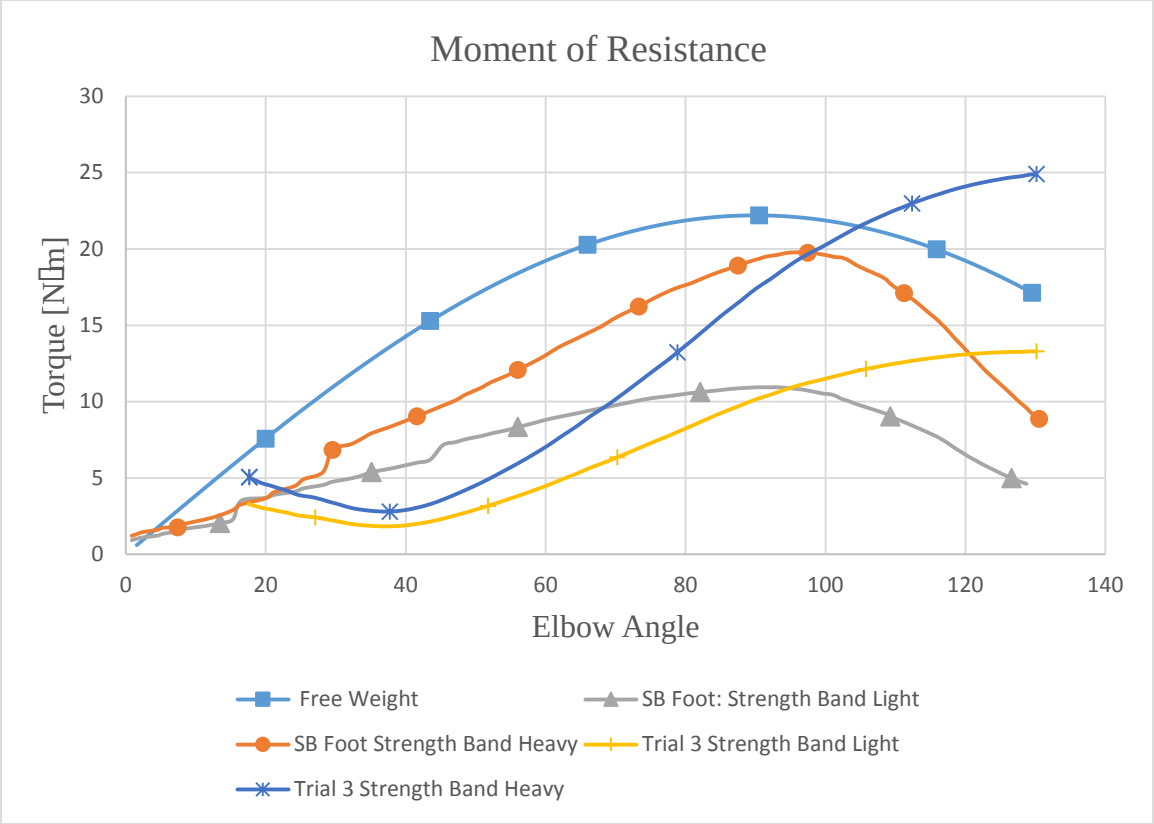

Figure 41: Comparison of the moment of resistance for FW, SB Foot, and SB Floor.

The moment of resistance during each trial can be seen in Figures 38-41**.** The moment of resistance is of critical importance since its optimization is key to the muscle forces being produced during an exercise. There was a large difference between all of the types of resistance tested. The free weight had the largest moment of resistance from elbow angles of 4.5□ to 104□. Both of the strength band's moments during Trial 2 (SB Foot) increase exponentially until an elbow angle of approximately 97.7□. After that, they exponentially decrease until 130□ of elbow flexion. When the strength band's attachment point is fixed 1 foot in front of the subject, the peak moment of resistance occurs at 130□ of elbow flexion.

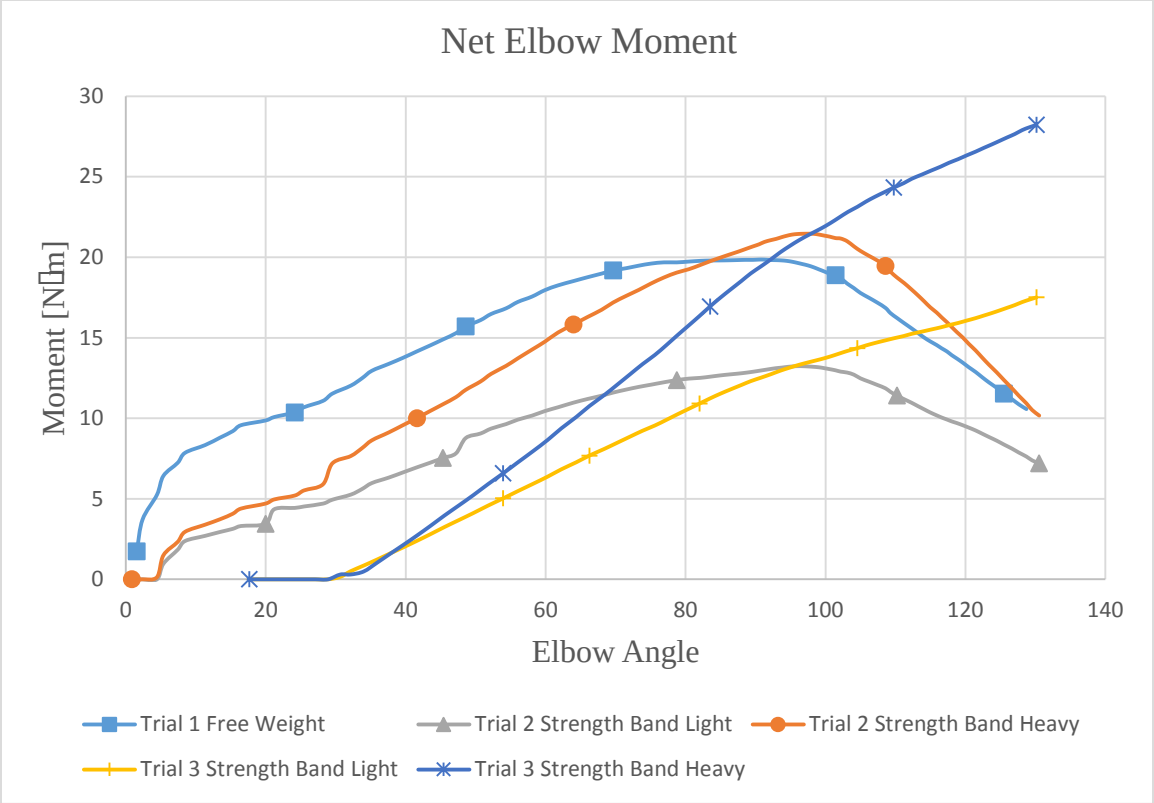

Figure 42: ID solutions exported from OpenSim of FW, SB Foot, and SB Floor with the five different external loads applied to the model.

The net elbow moment of each trial with the external loads applied to the OpenSim model can be seen in Figure 42. The net elbow moments for Trials 1 (FW) and 2 (SB Foot) all behave similarly. The elbow moment started low, hit a peak somewhere in between 80□ and 100□ of elbow flexion, and then decreased from the peak to 130□ of elbow flexion. Trial 3 (SB Floor) shows that the net elbow moment increases during the entire exercise. The net elbow moment is the highest during Trial 3 (SB Floor), and shows that the net elbow moment increases during the entire exercise. It should be emphasized that, prior to the exercise, the subject was told to complete the exercise without changing their speed of flexion. In other words, they were told to keep the resistance moving at a constant speed. The inverse dynamics solutions found in this study

are comparable to the results found by Pontonnier and Dumont (2009) in that the net elbow joint moment tends to be higher at the end of the motion than at the beginning.

Muscle force predictions for Trial 1 (FW) with the application of the free weight resistance to the model can be seen in Figures 43-45. The maximum potential muscle force was plotted along with the muscle force predictions using Equations 24 and 25 as the objective functions.

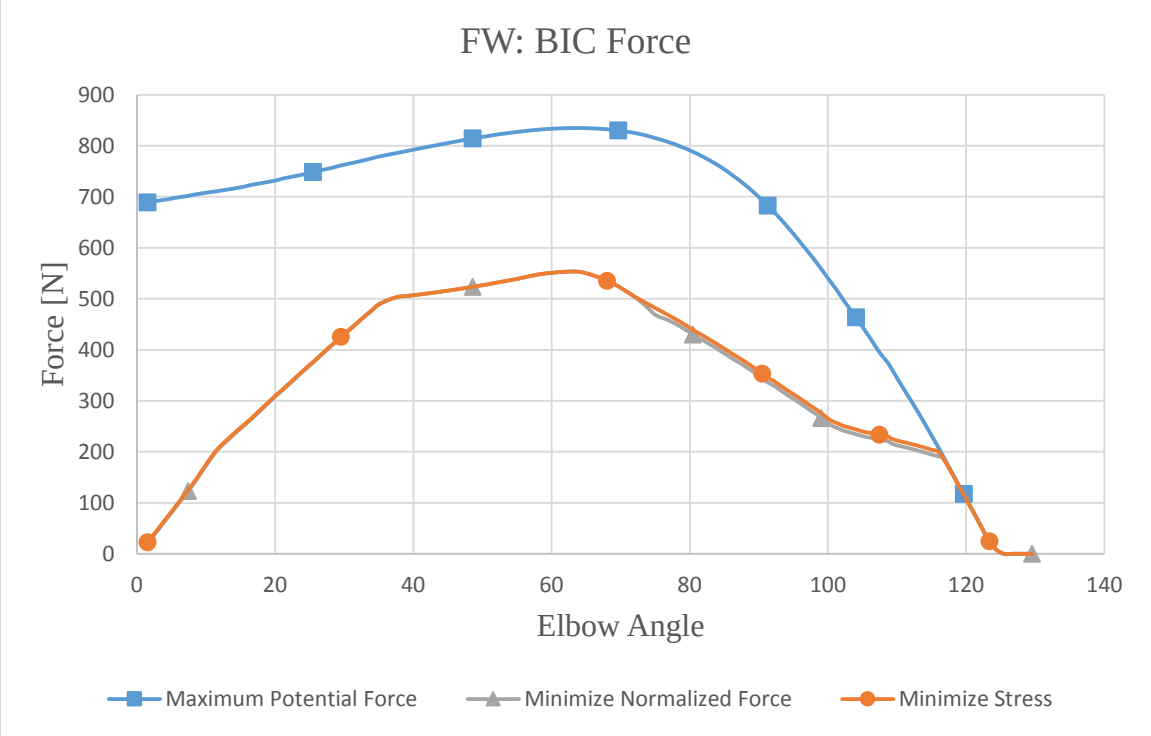

Figure 43: Comparison of the BIC maximum potential force and the predicted BIC force values for Trial 1 (FW) using Equations 24 and 25 for the objective functions.

By minimizing muscle stress, the optimization method predicted a slightly higher force in the BIC. However, the results match very well, and the difference in muscle forces between the two objective functions never exceeded 10 N. Both objective functions predict minimal muscle force at the beginning of the exercise and maximal muscle force at the end of the exercise when compared to the BIC maximum potential

force. At the beginning of the exercise the BIC has a maximum potential force of 690.9 N, but the muscle is only activated to produce 22.6 N of force. At the end of the exercise, the both objective functions predict that the BIC will be maximally activated to complete the exercise. The relationship between maximum potential force and muscle force is of paramount importance. It should be noted that if the subject wants to work his or her muscle effectively, one has to take advantage of the muscle's full capability. This will be discussed in more detail in Chapter 6.

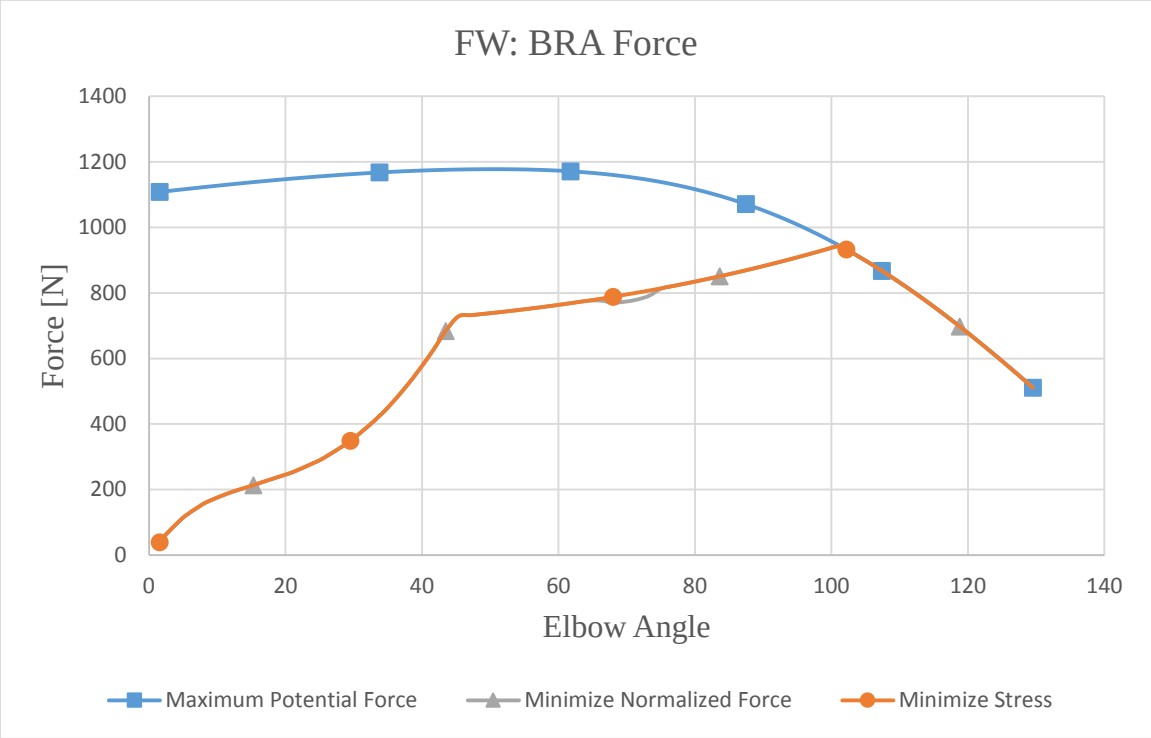

Figure 44: Comparison of the BRA maximum potential force and the predicted BRA force values for Trial 1 (FW) using Equations 24 and 25 for the objective functions.

Both objective functions predicted almost identical results for the BRA in Trial 1 (FW). By minimizing muscle stress, the optimization method predicted slightly lower BRA forces during the exercise. The difference between the two objective functions never exceeded 10 N. Overall, both objective functions predicted the BRA to

be minimally activated at the beginning of the exercise and maximally activated at the end of the exercise.

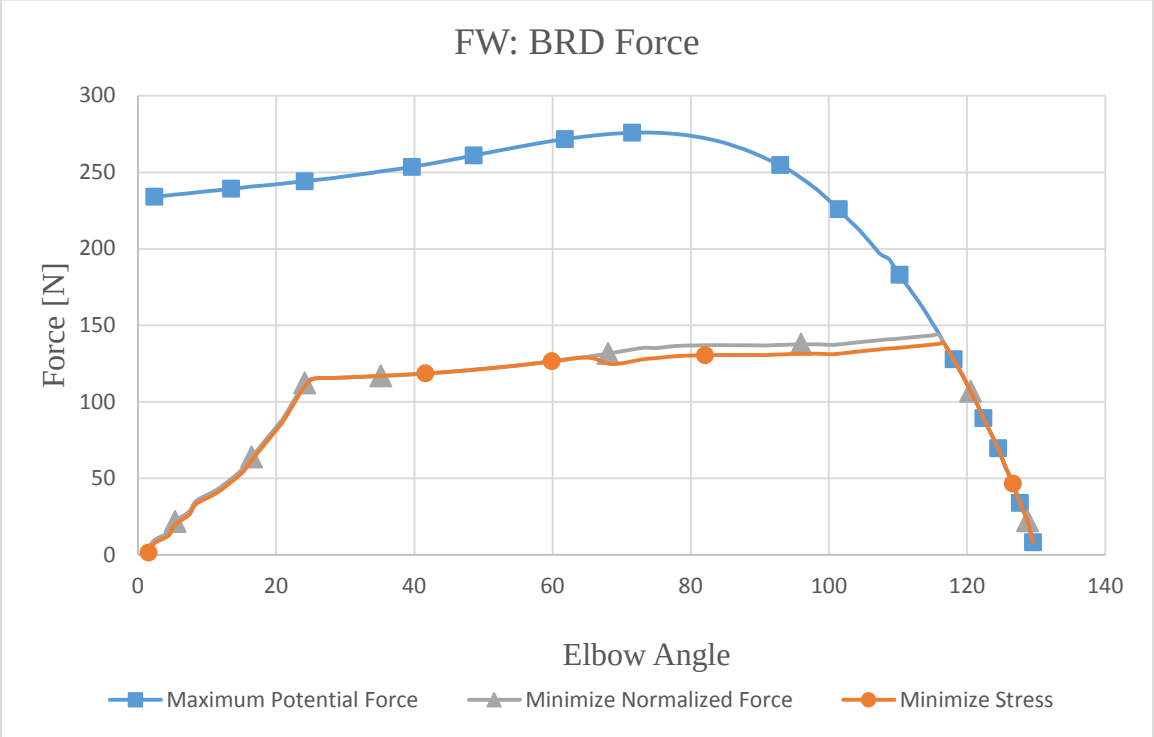

Figure 45: Comparison of the BRD maximum potential force and the predicted BRD force values for Trial 1 (FW) using Equations 24 and 25 for the objective functions.

Both objective functions predicted similar forces for the BRD in Trial 1 (FW). By minimizing stress, the optimization method predicted slightly higher forces for the BRD. The difference between the two objective functions never exceeded 10 N. Overall, the optimization method predicted the BRD to be minimally activated at the beginning of the exercise and maximally activated at the end.

Muscle force predictions for Trial 2 (SB Foot) with the application of the light strength band and heavy strength band resistances to the model can be seen in Figures 46-48. The maximum potential muscle force is plotted along with the muscle force predictions using Equations 24 and 25 as the objective functions.

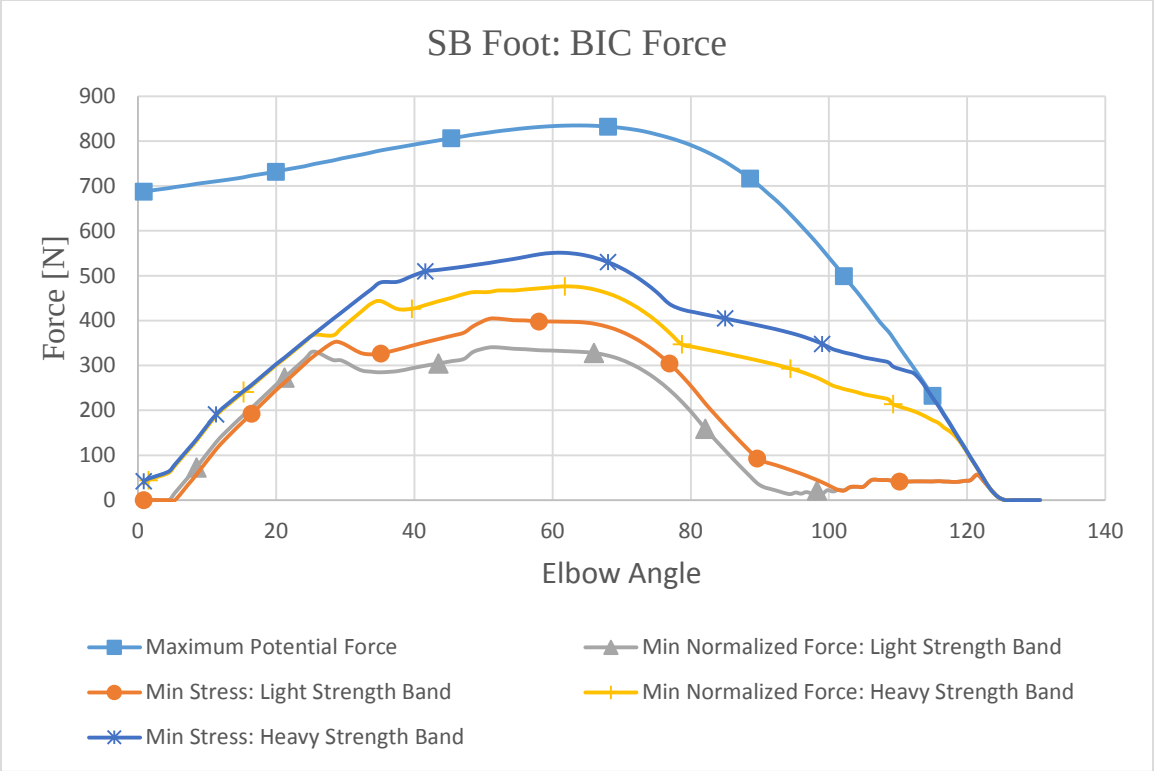

Figure 46: Comparison of the BIC maximum potential force and the predicted BIC force values for Trial 2 (SB Foot) using Equations 24 and 25 for the objective functions.

By minimizing the muscle stress, the optimization method predicted higher forces in the BIC when compared to those predicted by minimizing the normalized muscle force. The difference between the two objective functions is at a maximum of 64.2 N at an elbow angle of 52.2° when using the light strength band, and 74.6 N at an elbow angle of 64.0°. Peak BIC force values are predicted to occur between elbow joint angles of 52.2° and 64.0°. As in Trial 1 (FW), the BIC is predicted to be minimally activated at the beginning of the exercise and maximally activated at the end with the use of the heavy strength band. The BIC force drops off considerably after 80° of elbow flexion when using the light strength band.

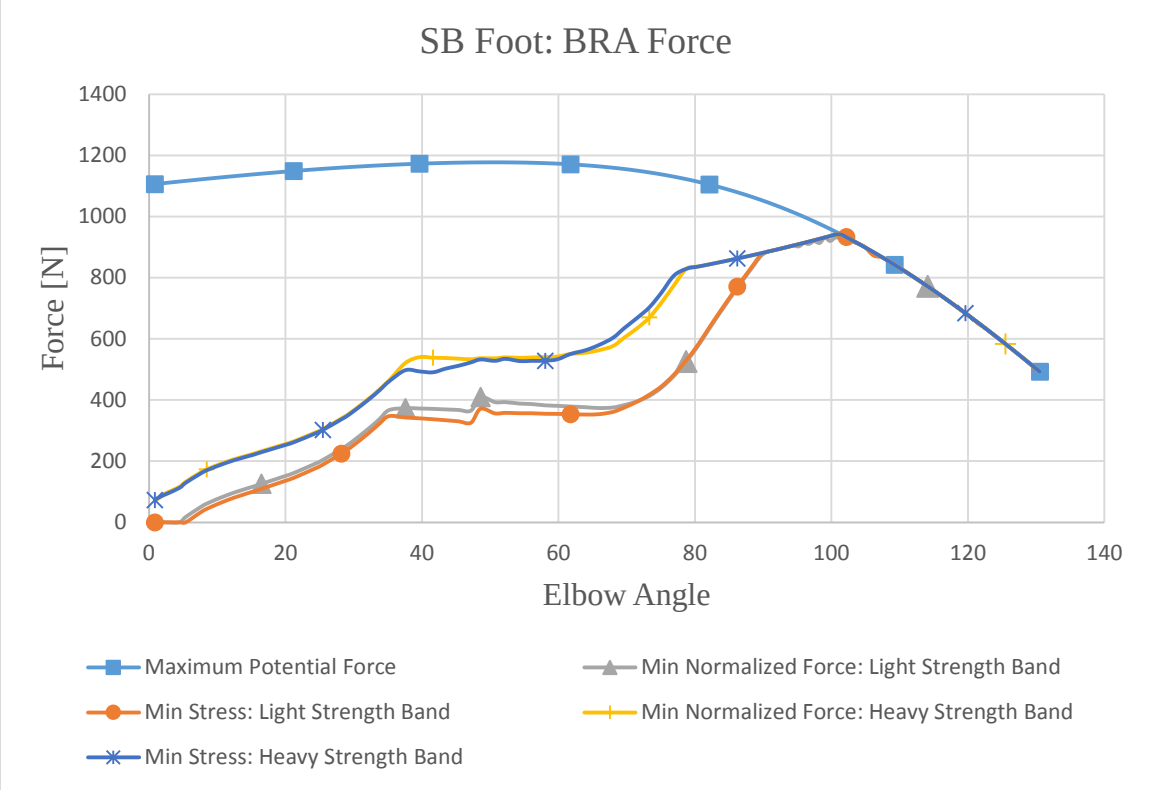

Figure 47: Comparison of the BRA maximum potential force and the predicted BRA force values for Trial 2 (SB Foot) using Equations 24 and 25 for the objective functions.

By minimizing the muscle stress, the optimization method predicted lower forces in the BRA when compared to those predicted by minimizing the normalized muscle force when using the light strength band. However, when the heavy strength band was applied to the model and normalized force was minimized, the BRA was predicted to have a higher force in the range of 35.2° to 61.8° of elbow flexion than when muscle stress was minimized. At elbow joint angles of 61.8° to 78.7°, it was the opposite. Overall, as in Trial 1 (FW), the BRA is predicted to be minimally activated at the beginning of the exercise and maximally activated at the end of the exercise. Overall, the BRA force increases during the entire exercise until it reaches its peak limit at 102° of flexion.

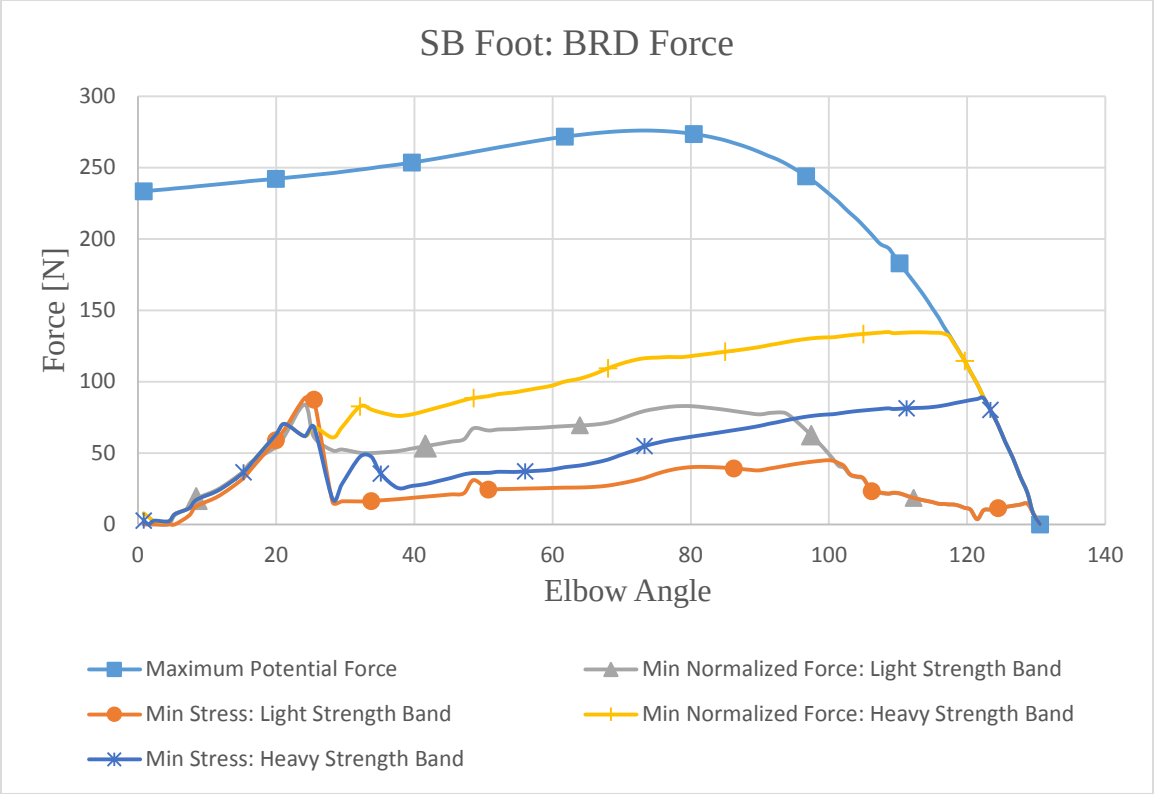

Figure 48: Comparison of the BRD maximum potential force and the predicted BRD force values for Trial 2 (SB Foot) using Equations 24 and 25 for the objective functions.

By minimizing normalized muscle force, the BRD force was predicted to be significantly higher while using both strength bands. As in Trial 1 (FW), the BRD was predicted to be minimally activated at the beginning of the exercise and maximally activated at the end.

Muscle force predictions for Trial 3 (SB Floor) with the application of the light strength band and heavy strength band resistances to the model can be seen in Figures 49-51. The maximum potential muscle force was graphed along with the muscle force predictions using Equations 24 and 25 as the objective functions.

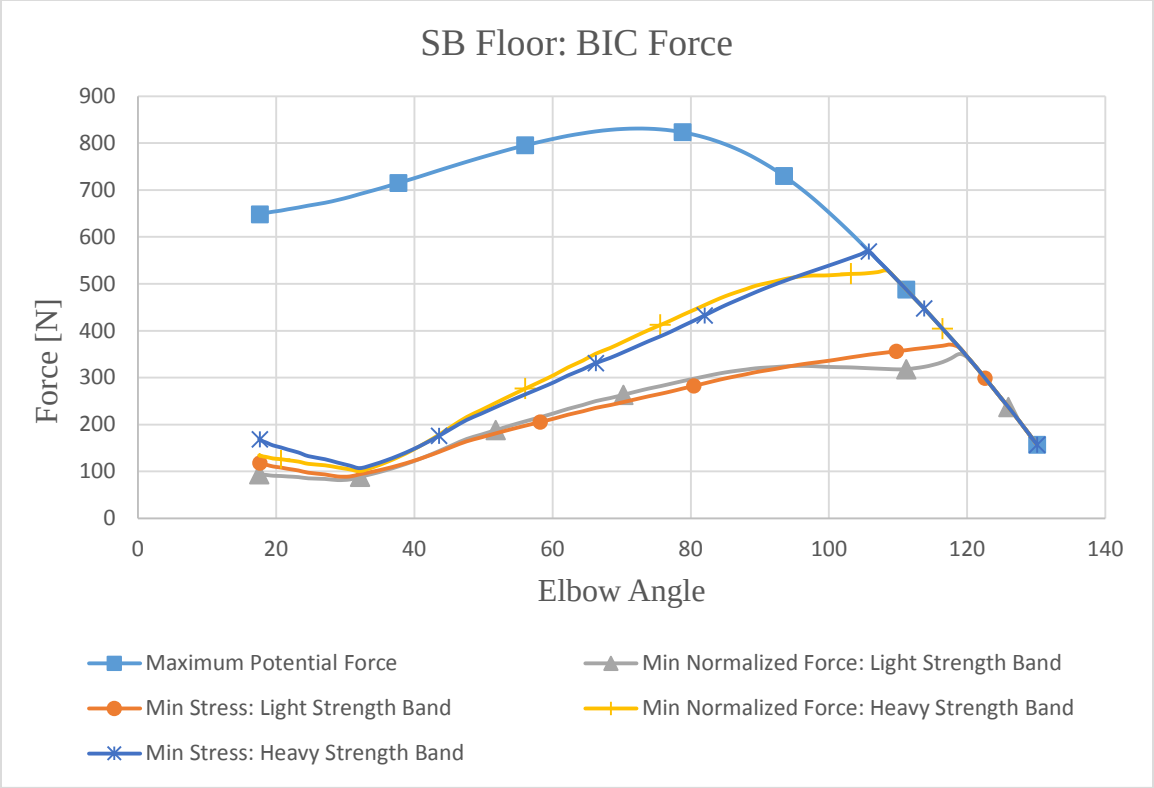

Figure 49: Comparison of the BIC maximum potential force and the predicted BIC force values for Trial 3 (SB Floor) using Equations 24 and 25 for the objective functions.

The BIC force predictions were very similar between the two objective functions. The BIC force decreased from elbow angles of 17.9 to 32 of elbow flexion. Then it steadily rose for the rest of the exercise until it hit its maximum potential force at the end of the exercise. Trial 3 (SB Floor) predicted that the BIC would be minimally activated at the beginning of the exercise and maximally activated at the end.

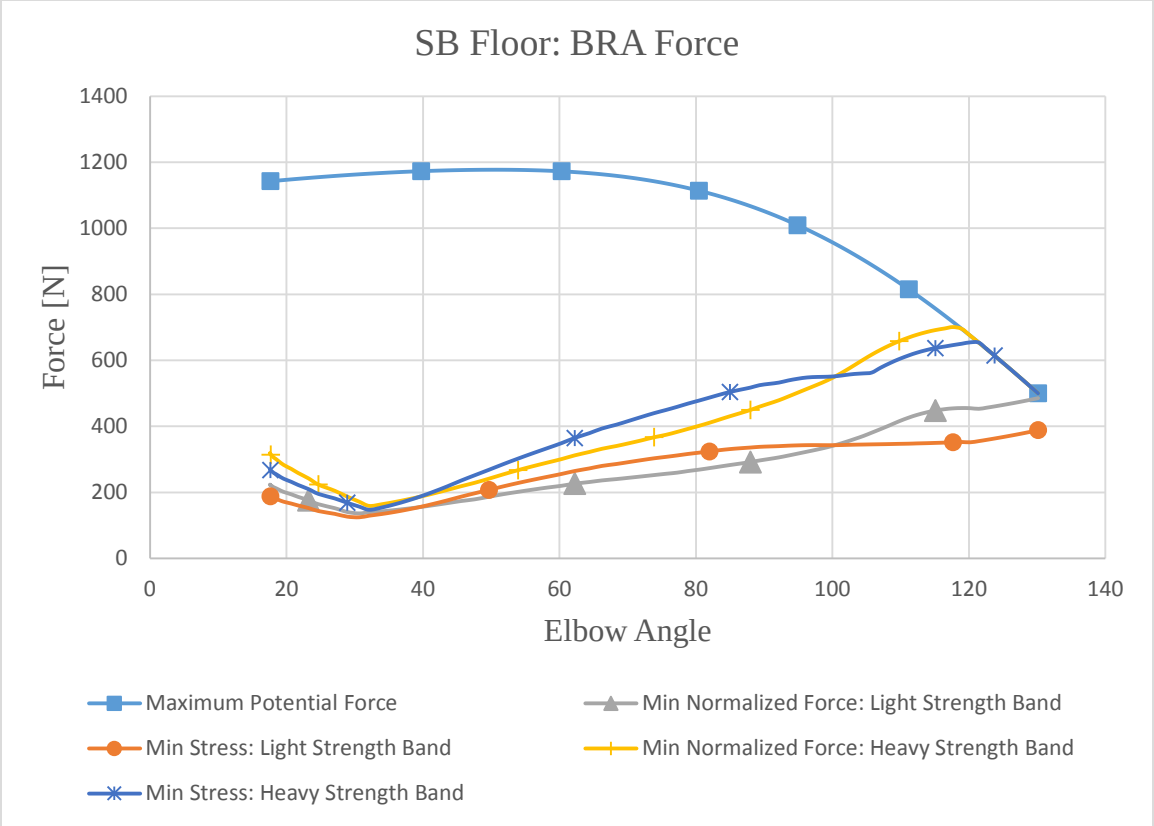

Figure 50: Comparison of the BRA maximum potential force and the predicted BRA force values for Trial 3 (SB Floor) using Equations 24 and 25 for the objective functions.

The BRA force predictions were very similar between the two objective functions. The BRA force decreased from elbow angles of 17.9° to 32° of elbow flexion. Then it steadily increased for the rest of the exercise until it hit its maximum potential force at the end of the exercise. When using the light strength band, the BRA never hit its maximum potential, but its force was still higher at 130° of elbow flexion than at any other joint angle. Trial 3 (SB Floor) predicted that the BRA would be minimally activated at the beginning of the exercise and maximally activated at the end.

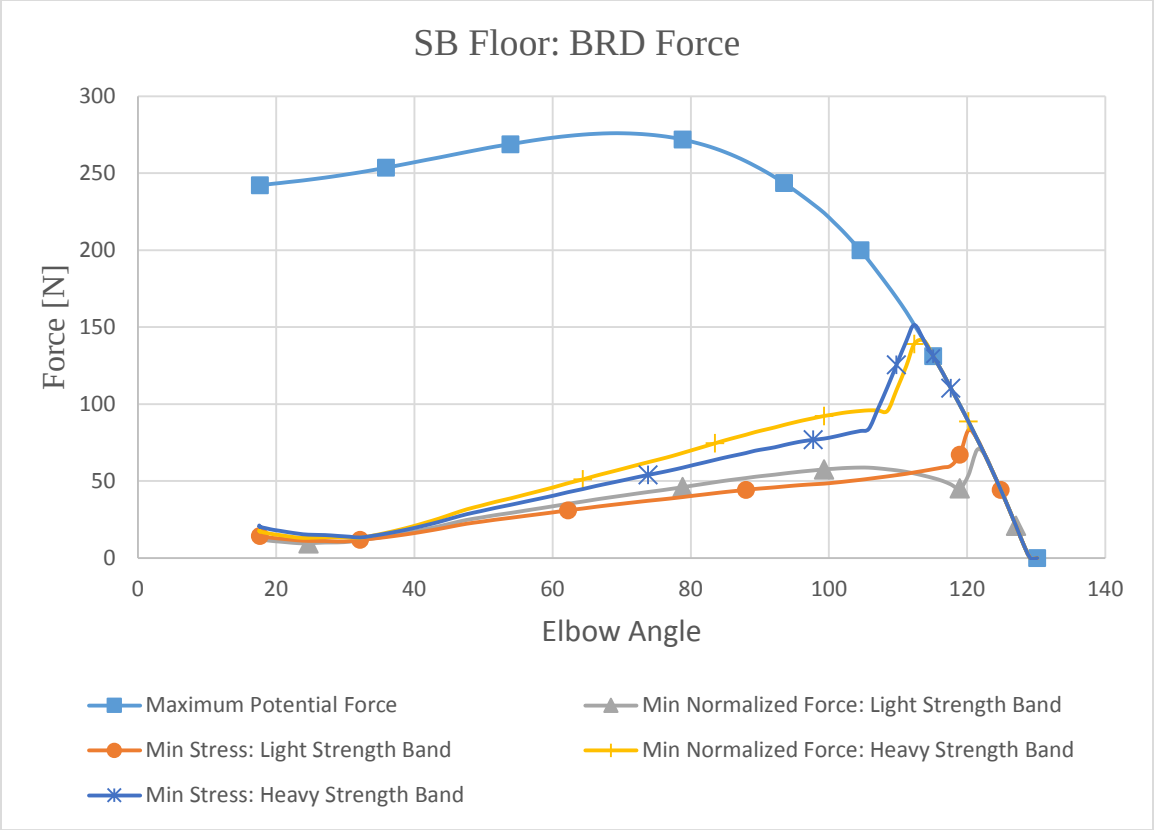

Figure 51: Comparison of the BRD maximum potential force and the predicted BRD force values for Trial 3 (SB Floor) using Equations 24 and 25 for the objective functions.

The BRD force predictions were very similar between the two objective functions. The BRD force decreased from elbow angles of 17.9° to 32° of elbow flexion. Then, it steadily increased for the rest of the exercise until it spikes at 107.1° with the heavy strength band and 122.3° with the light strength band. Trial 3 (SB Floor) predicted that the BRA would be minimally activated at the beginning of the exercise and maximally activated at the end.

CHAPTER 6: DISCUSSION

The results of this study prove that current forms of resistance do not exercise skeletal muscle to its full capability. The resistance moment is at its highest when the muscle's maximum potential force is at its lowest. In general, a strength band's resistance increases as the exercise is performed. This is counter-productive. There is so much potential muscle force that is not being taken advantage of at the beginning of the exercise. The optimized moment of resistance is determined for in this chapter that will exercise skeletal muscle to its full capability, thus, saving the user time and exercising the muscles more effectively.

6.1. It was found in this study that forearm pronation/supination has a huge effect on the maximum potential force of the BIC and BRA. Supination of the forearm will cause the BIC's peak force to occur earlier in the curl motion and cause the BRD's peak force to occur later in the motion. In order to design exercise equipment, we have to know where the muscles are at their strongest and then increase the moment of resistance at these points while decreasing it where the muscles are weak. Shoulder elevation and rotation do not have as drastic of an effect on the BIC, but still affect it. It was found in this study that in order to design effective exercise equipment, the equipment has to be widely adjustable. The equipment has to be able to change according to different exercises. For example, a simple change of forearm rotation drastically changes where the BIC and BRA maximum force occurs during a curl. The ideal exercise equipment should be able to adjust the moment of resistance that it is applying to the hand.

6.2. The muscle moment arm curves are important because they dictate how much torque a muscle can generate. There were no significant changes in the BIC and BRA moment arms between the three exercises. However, there was a change in the BRD moment arm when using the strength band attached 1 foot in front of the subject. The attachment point of the BIC and BRA moves in an arc around the elbow joint center. This is important because it affects how much torque each of these muscles can generate in order to flex the elbow joint. As the moment arm becomes smaller, so will the maximum torque that the muscle can generate. Even though the BIC and BRA moment arms are at their largest at 109 of flexion, it does not mean this is where maximum torque generation occurs. It simply means that more torque can be generated with less force. It is important to note that Figure 30 shows that the decreased supination angle has an effect on the BRD

moment arm. In Trial 3 (SB Floor), the BRD has a bigger moment arm than in Trials 1 (FW) and 2 (SB Foot). This, combined with the results found in Figure 25 tells us that the BRD is highly susceptible to forearm pronation/supination. How joint angles affect a muscle's moment arm must be taken into consideration when designing an optimized form of resistance because the moment arm directly affects the muscles RTG and where the peak of the maximum torque curve will occur. The moment arm's progression through the movement reported in this study do not agree with the results reported by Pigeon et al. (1996) and Amis et al. (1979). The subjects that were tested were different in all of the studies, but this should be an area of further research that could help physicians when they are considering moving the attachment point of certain muscles.

The moment arm of the three different types of resistance are of paramount importance because it directly affects the moment of resistance on the elbow joint. Figure 31 shows that the resistance in Trial 2 (strength band attached at the foot) has the largest moment arm from 0° to 52.2° of elbow flexion. This is good when trying to optimize the resistance because this is the range where all of the muscles are at their strongest. A bigger moment arm means, potentially, a bigger moment of resistance. Where the strength band fails is that even though the moment arm is large at the beginning of the exercise, the tension in the band is low. Trial 3 (SB Floor) shows that this exercise is the worst out of the three exercises. The moment arm is small at the beginning of the exercise and is large at the end. From Figure 31, it can be seen that the moment arm of the resistance can be easily changed throughout the exercise. This makes it an effective tool when trying to change the moment of resistance that the exercise equipment is applying.

The moment arm of the resistance was taken into account when designing the ideal exercise equipment.

The maximum torque that a muscle can generate is not constant throughout joint rotation. It depends on the maximum potential force and moment arm of the muscle. Figures 24 and 36 show that neither of the exercises or forearm pronation/supination have an effect on the BRA maximum torque curve. As expected, forearm pronation/supination has an effect on the BIC and BRD maximum torque curves. Figures 38-40 show that none of the exercises are taking full potential of the elbow flexors' capability. In every trial, the resistance moment starts low and ends high. In Trials 1 (FW) and 3 (SB Foot) the elbow flexors' are being maximally activated at the end of the exercise. It can be determined from Figures 38-40 that a good place to start when designing exercise equipment would be to aim to achieve a moment of resistance that is related to the maximum elbow torque curve. For example, when the elbow torque curve peaks, it would be ideal for the moment of resistance to peak as well. The moment of resistance should be directly proportional to the maximum elbow torque.

Figures 43-51 show that the choice of the objective function does matter. By minimizing normalized muscle force, the optimization method consistently predicted that the BIC force would be lower and the BRD force would be higher than when muscle stress was minimized. The BIC has a much larger volume than the BRD. Therefore, it can handle more tension. This would explain why the optimization method predicted that the BIC forces would be higher when minimizing muscle stress. The BRA is affected by the choice of objective function, but the effects on it are based more on what the force for the BIC and BRA are. Overall, both objective functions produce similar results for the three

different exercises. Muscles are predicted to be minimally activated at the beginning of the exercise and maximally activated at the end. The results are so similar that both objective functions are useful and accurate to use when calculating muscle forces.

Figures 43-51 prove that current forms of exercise do not exercise skeletal muscle effectively. Maximum force for the three muscles tends to occur at approximately 64.0°, 50.7°, and 73.3° of elbow flexion for the BIC, BRA, and BRD. These results do not agree with the results found by An et al. (1989) who assumed that all elbow flexors peak around 78° of flexion. In Trial 1 (FW), all muscles are minimally activated at the beginning of the exercise and maximally activated at the end. This can be attributed to the moment created by the free weight. It is low at the beginning of the exercise and high at the end as can be seen in Figure 41. In order to take advantage of the unused potential force at the beginning of the exercise, the moment of resistance must be higher. Furthermore, the moment of resistance is too high at the end, and this is where the muscles are at their weakest. By doing this exercise, the user is putting forth maximum effort at the end and minimal effort at the beginning. It would be more effective to work the muscle at a set portion of its maximum potential force. For example, if the user wants to work their muscles at 50% of their maximum force. The moment of resistance would have to be higher at the beginning of this exercise and lower at the end in order to ensure that the muscle is worked effectively at every joint angle.

In Trial 2 (SB Foot), Figures 46-48 show similar results to Trial 1 (FW). At the beginning of the exercise the muscles are minimally activated. Ideally, the muscles need to be working harder at this elbow angle because there is so much potential muscle force that is not being used. Furthermore, the muscles all become maximally activated at the

end of the exercise. Once again, the exercise did not take full advantage of the available muscle force.

In Trial 3 (SB Floor), Figures 49-51 show that this is the worst exercise out of the three for skeletal muscle. All of the muscle force predictions follow the same pattern. They are minimally activated at the beginning of the exercise and maximally activated at the end. By moving the strength band's attachment point forward, the exercise is less effective than when the attachment point is at the subject's foot. Ideally, the muscle force curve should follow the maximum muscle force curve proportionally. Where the BIC, BRD, and BRA are strongest, the moment of resistance was at its lowest. At elbow joint angles of 105° to 130° the moment of resistance is at its highest. It was not because the strength band was stretched that much further. The bigger moment caused by the strength band was due to the dramatic increase in its moment arm. This reinforces the idea that the moment of resistance can be effectively controlled by changing the resistance moment arm.

The goal of this study was to gain evidence towards the design of better exercise equipment that will work skeletal muscle more effectively. From the results, it can be seen that the root of the problem lies in the moment of resistance. In general, current forms of exercise apply too little load at the beginning of the exercise and too much at the end. So, how can it be fixed? There are two ways to control the moment of resistance. The first is by modifying the resistance moment arm during the exercise. The second is to modify the force of the resistance. Ideally, the exercise equipment should work the opposite way that the strength band works. The resistance magnitude should be high at the beginning and low at the end. This is hard to do.

Nautilus machines modified the moment of resistance successfully with the use of a cam wheel, and the same type of wheel can be found on a compound bow.

Figure 52: Example of a cam wheel used by Nautilus machines and compound bows.

Studies by Harman (1983) and Cabell and Zebas (1999) have shown little correspondence between the machine resistive torque (MRT) that these machines apply and human torque capability (HTC). Both studies show a significant difference between HTC and MRT at the extreme positions of the elbow. Harman (1983) reported values of up to 59% difference between HTC and MRT at the extreme positions. Furthermore, these types of machines can only be designed for one size of person. They cannot be customized or changed to fit the physiological parameters of everyone. The machine may be designed to match the angular-torque relationship of the 50^{th} percentile male. However, the machine will not be effective for a man that is 6’3”. There would have to be a different cam for every different size of person.

In order to find what the moment of resistance curve should be, the kinematic motion from Trial 3 (SB Floor) was used to obtain an inverse dynamics solution with no resistance and used as the target net elbow moment. This was done for two reasons. The first is that most exercise equipment that could be designed would involve some form of cable or band that is attached to a machine. The second is that there were no prototypes of newly designed exercise equipment that could be used as the resistance during motion capture. So, a 'target' net elbow moment had to be set. The net elbow moment can be set to whatever the user wishes. The net elbow moment generated with no resistance can be used because this ensures that the exercise motion will be a smooth motion. Next, Equation 27 was used to solve for the optimized moment of resistance.

$$a(F_{BIC,M}\, r_{BIC} + F_{BRA,M}\, r_{BRA} + F_{BRD,M}\, r_{BRD}) + F_{forearm}\, r_{forearm} + M_R = M_{net} \quad (27)$$

Where a is the activation level, $F_{BIC,M}$ $F_{BRA,M}$ $F_{BRD,M}$ are the maximum values of the BIC, BRA, and BRD, M_R is the optimized moment of resistance to be found, and $M_{net}$is the net elbow moment. a was chosen to be 0.5 in this calculation. It should be noted that a can be set to any number between 0 and 1. For example, if the user wants to work the muscles to 75% of their maximum potential, then a would be 0.75. The optimized moment of resistance is reported in Figure 53.

Figure 53: Moment of resistance curve for the Trial 3 (SB Floor) kinematic motion.

Once the optimized moment of resistance was calculated, an external load file was made and applied to the OpenSim model using inverse dynamics. From there, static optimization was ran to test the optimized moment of resistance and see how effectively it works the muscles. The results are reported in Figures 54-59.

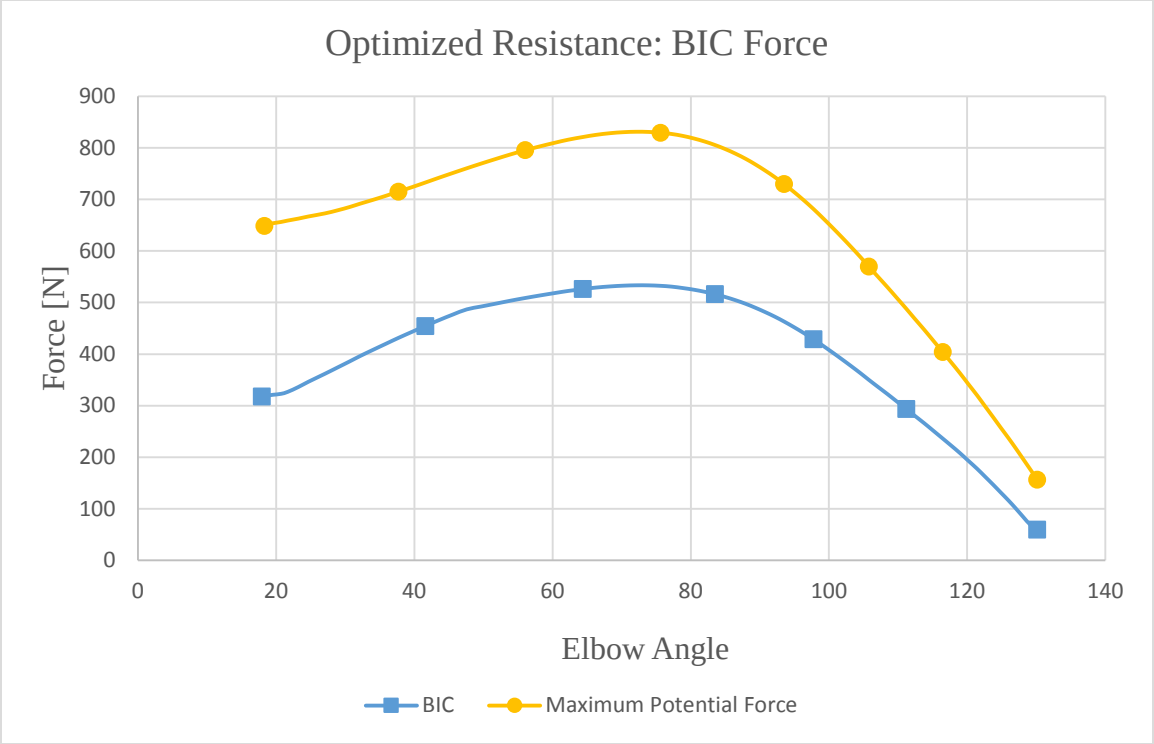

Figure 54: Comparison of the BIC max force curve to the predicted BIC force values using static optimization with the application of the optimized moment of resistance.

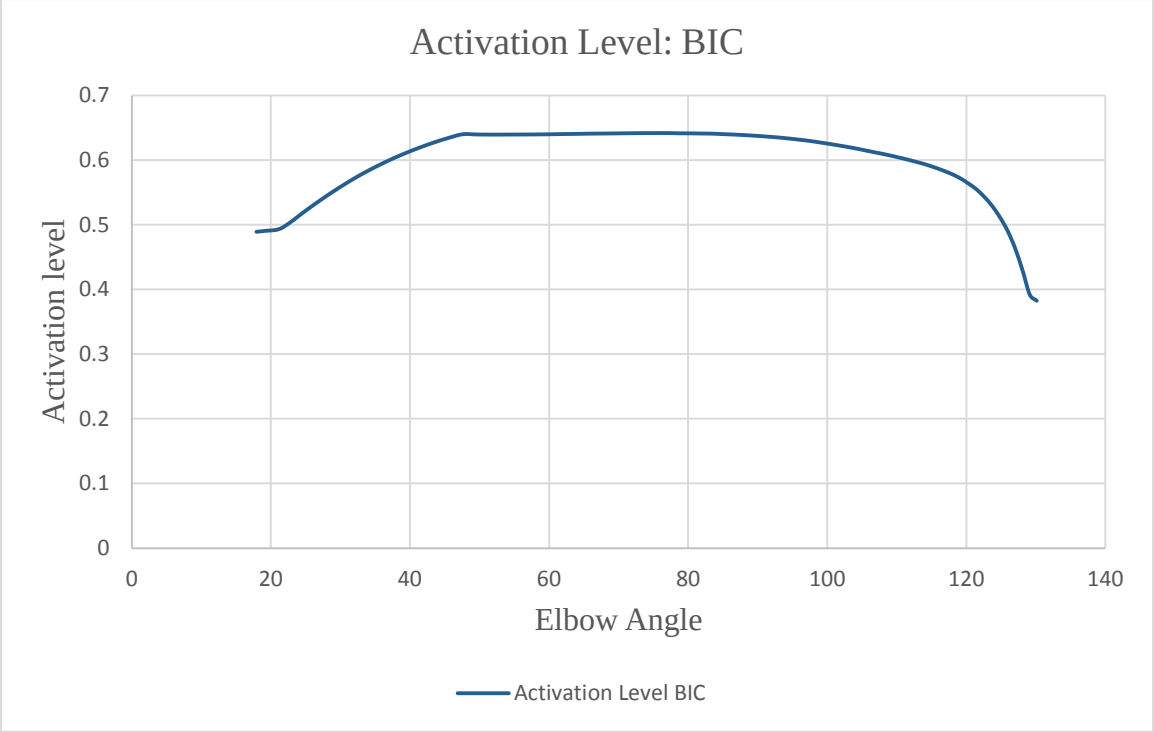

Figure 55: Activation level of the BIC with the application of the optimized moment of resistance.

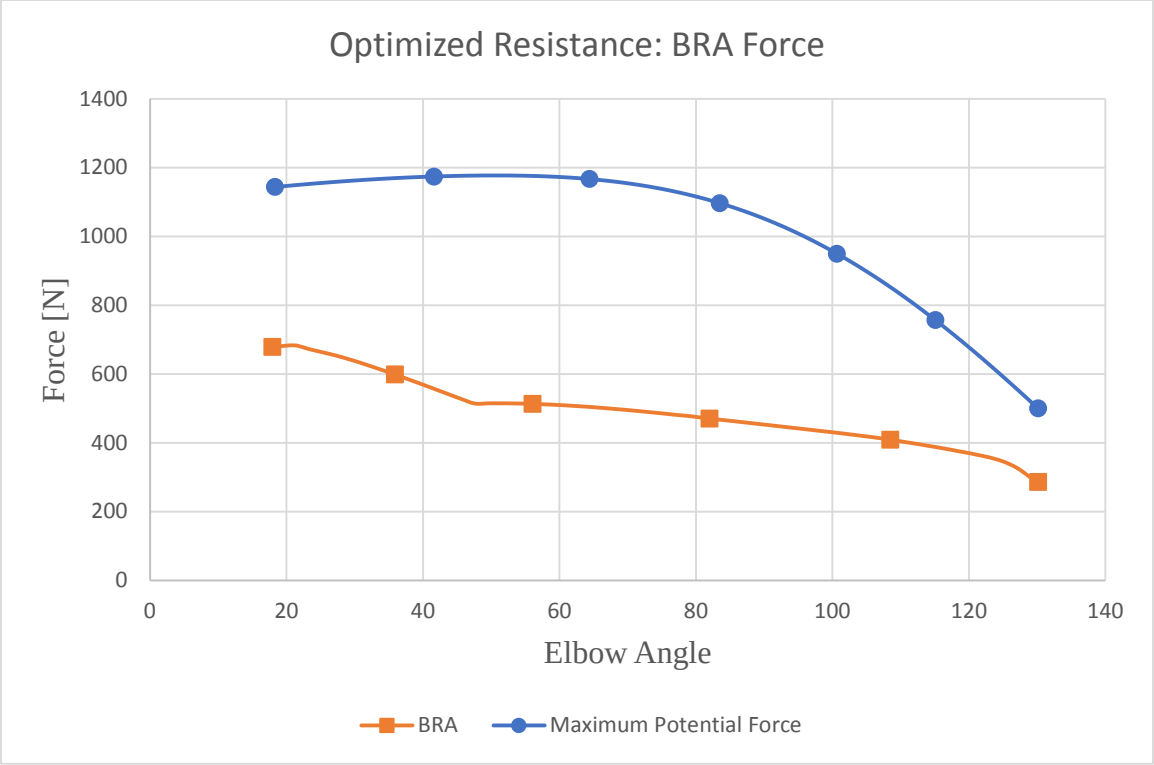

Figure 56: Comparison of the BRA max force curve to the predicted BRA force values using static optimization with the application of the optimized moment of resistance.

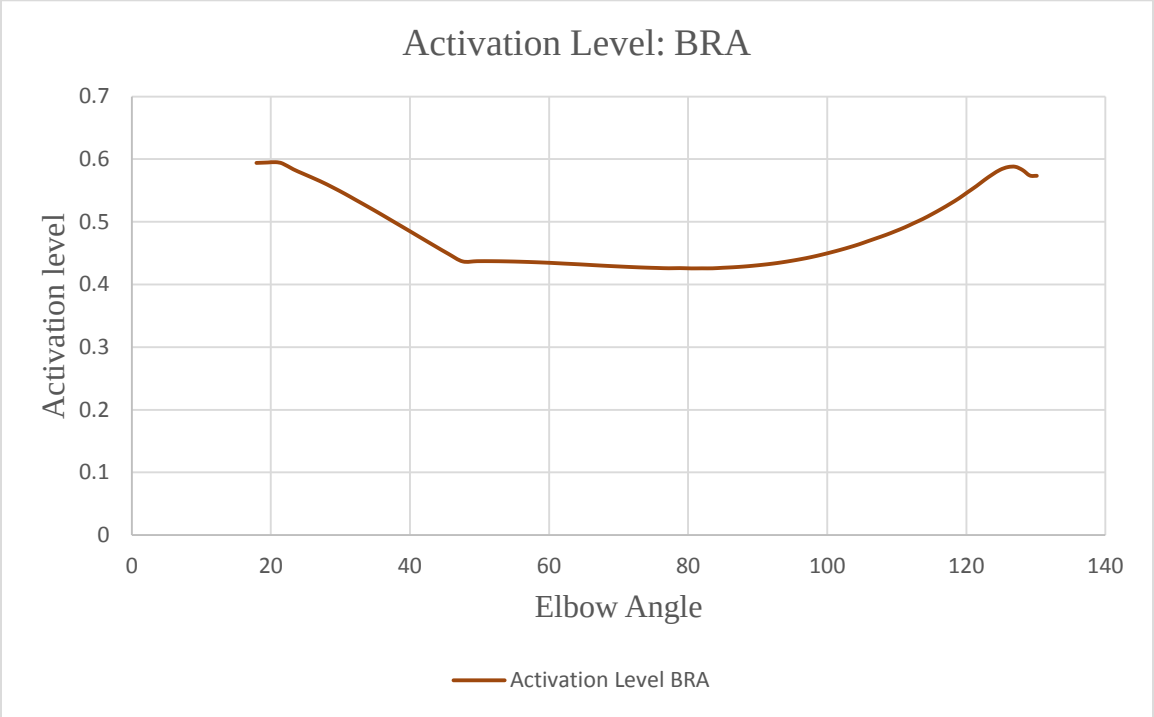

Figure 57: Activation level for the BRA with the application of the optimized moment of resistance.

Figure 58: Comparison of the BRD max force curve to the predicted BRD force values using static optimization with the application of the optimized moment of resistance.

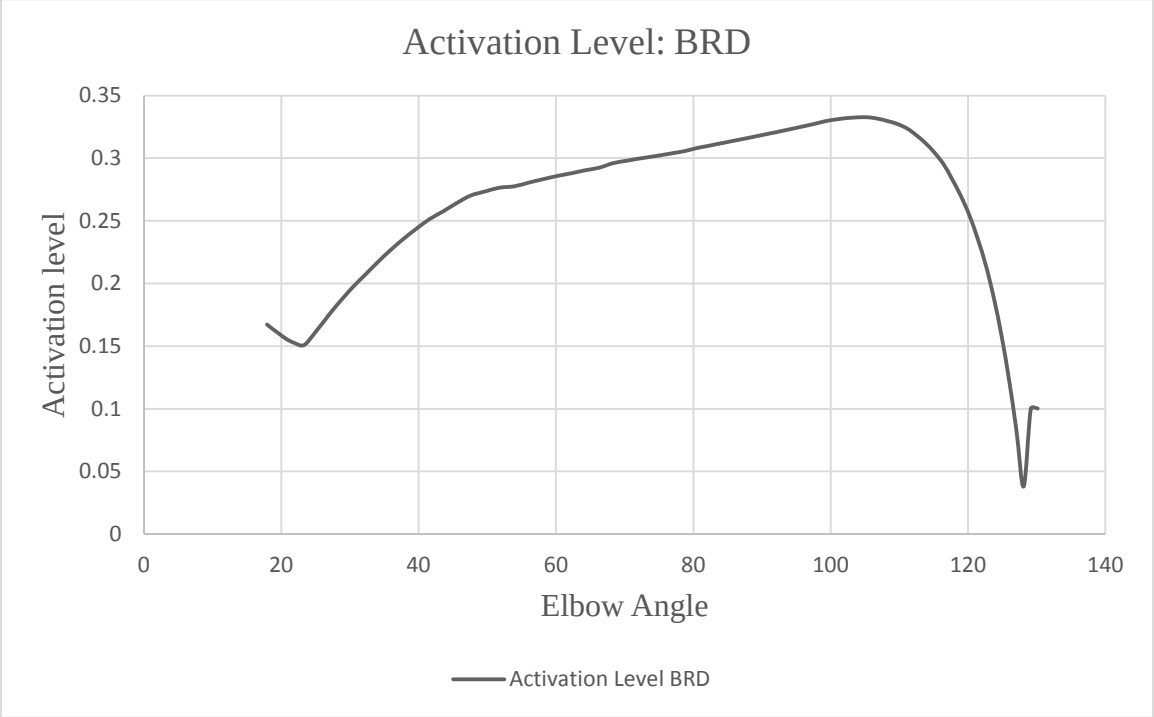

Figure 59: Activation level for the BRD with the application of the optimized moment of resistance.

The results show that the optimized moment of resistance is much more effective than the free weight or strength band. The best results are in Figure 56 and 57. The predicted force of the BRA is an average of 49.2% of the maximum force for the entire exercise. Overall, Figures 54, 55, 58, and 59 show promising results. The muscles are producing more force at the points when they are at their strongest. The results show that the muscles are being worked more effectively during the exercise. However, the values are not exactly 50% of their maximum. The BIC activation level is around 50%, but varies from a low of 38.3% to a high of 63.0%. The reason that the muscles are not exactly activated at 50% is due to how the optimization method solved for the muscle forces. The BRD activation level is so low because in order to minimize the objective function the BRD has to have a low value. This results in higher values for the BIC and BRA. The results show that the moment of resistance cannot be based purely off of the maximum torque curve of the elbow joint. In general, this is a good start at calculating what the optimized moment of resistance should be, but additional work is required in order to optimize it to perfection. The first improvement that should be made is the addition of the velocity-force relationship to the model. The velocity of contraction will have a direct effect on the maximum potential force of each muscle. Second, the objective functions should be derived to take into account multiple objectives. For example, the static optimization method should include the minimization of stress and normalized force at one time.

Further modification to the objective function could also be of benefit. (Raikova (1996)) proposed that weight coefficients can be given to the muscles. This could be useful when analyzing motion post-surgery. If the attachment point of the BIC is

changed, then higher weight coefficients could be given to the BRA and BRD in order to simulate movement more accurately. Future work could also include simply using this optimization method to apply different magnitudes of resistance to an existing exercise. It would be useful to perform the exercise with a cable machine, calculate the cable's moment arm, and then test different magnitudes of resistance to see how they work the muscles. By doing this, insight can be gained as to possible designs that use an existing machine with the addition of some mechanism that will vary the magnitude of the resistance as the exercise is performed. It would also be ideal to have a prototype built to test using the optimization method. Using a prototype would lead to a more realistic net elbow moment during the kinematic motion. The results in this study show that there is a need for better designed exercise equipment, as well as, providing an optimized moment of resistance to match.

CHAPTER 7: CONCLUSION

Three different exercises with two different forms of resistance were evaluated on how well they exercise the elbow flexors during a curl. The forms of resistance tested were a free weight and a strength band. The curl was performed in three different ways. The first exercise was performed with the free weight, the second with the strength band attached at the foot, and the third with the strength band attached to the floor 1 foot in front of the subject. The results show that none of the exercises tested are effective in working the elbow flexors to their full capability.

Motion capture data was imported to OpenSim where key muscle parameters were exported to a customized MATLAB script. From there, static optimization was performed based on the physiological parameters of skeletal muscle in order to determine the individual muscle forces. The results show that none of the exercises work the muscles to their full potential. The moment of resistance was reported to be as low as 1 $N \cdot m$ at the beginning of the exercise with a maximum potential elbow torque of 22.4 $N \cdot m$. Furthermore, the moment of resistance at the end of the exercise consistently caused maximal muscle activation. This is contradictory to what is desired. The elbow flexors are at their strongest at the beginning of the curl motion and weakest at the end. Next, the optimized moment of resistance was calculated based on the maximum potential force that each muscle could exert at a given joint angle. The optimized moment provides a target moment of resistance for the design of better exercise equipment.

The novelty of this study is that it calculates muscle force based on multiple key physiological parameters. Other studies have used only a fraction of the parameters used here. Furthermore, the work done here calculates the muscle forces based on the previous state of the muscles and with an external load during an entire exercise. Other studies only optimize the muscle force during isometric contractions at one joint angle or with no external load at all. Future work should include the addition of the velocity-force relationship to this model and exploration of different objective functions. This model can be used to test theoretical moments of resistance and determine how well they exercise skeletal muscle. The work done in this study also provides insight to the future design of more effective exercise equipment.

In conclusion, the free weight and strength band have been proven to not work skeletal muscle to its full capability. The optimized moment of resistance has been solved for that will ultimately lead to shorter, more effective workouts. The evidence in this study can lead to an entire new generation of exercise equipment that can be customized to improve workout effectiveness.

REFERENCES

Aagaard, P., E. B. Simonsen, J. L. Andersen, P. Magnusson and P. Dyhre-Poulsen (2002). "Increased rate of force development and neural drive of human skeletal muscle following resistance training." Journal of applied physiology (Bethesda, Md. : 1985) **93**(4): 1318-1326.

Aguinaldo, A. L., J. Buttermore and H. Chambers (2007). "Effects of upper trunk rotation on shoulder joint torque among baseball pitchers of various levels." Journal of applied biomechanics **23**(1): 42-51.

Amis, A. A., D. Dowson and V. Wright (1979). "Muscle Strengths and Musculo-skeletal Geometry of the Upper Limb." Engineering in Medicine **8**(1): 41-48.

An, K., F. Hui, B. Morrey, R. Linscheid and E. Chao (1981). "Muscles across the elbow joint: a biomechanical analysis." Journal of biomechanics **14**(10): 659-669.

An, K. N., K. R. Kaufman and E. Y. Chao (1989). "Physiological considerations of muscle force through the elbow joint." Journal of biomechanics **22**(11-12): 11-12.

An, K. N., B. M. Kwak, E. Y. Chao and B. F. Morrey (1984). "Determination of muscle and joint forces: a new technique to solve the indeterminate problem." Journal of biomechanical engineering **106**(4): 364-367.

Andersen, L. L. and P. Aagaard (2006). "Influence of maximal muscle strength and intrinsic muscle contractile properties on contractile rate of force development." European journal of applied physiology **96**(1): 46-52.

Biewener, A. A., J. M. Wakeling, S. S. Lee and A. S. Arnold (2014). "Validation of Hill-type muscle models in relation to neuromuscular recruitment and force-velocity properties: predicting patterns of in vivo muscle force." Integrative and comparative biology **54**(6): 1072-1083.

Buchanan, T. S., D. G. Lloyd, K. Manal and T. F. Besier (2004). "Neuromusculoskeletal modeling: estimation of muscle forces and joint moments and movements from measurements of neural command." Journal of applied biomechanics **20**(4): 367-395.

Cabell, L. and C. J. Zebas (1999). "Resistive Torque Validation of the Nautilus Multi-Biceps Machine." The Journal of Strength & Conditioning Research **13**(1): 20-23.

Capozzo, A., F. Catani, A. Leardini, M. G. Benedetti and U. Della Croce (1995). "Position and orientation in space of bones during movement: experimental artefacts." CLINICAL BIOMECHANICS -BRISTOL- **11**(2): 90-100.

Challis, J. H. (1997). "Producing physiologically realistic individual muscle force estimations by imposing constraints when using optimization techniques." Medical Engineering and Physics **19**(3): 253-261.

Challis, J. H. and D. G. Kerwin (1993). "An analytical examination of muscle force estimations using optimization techniques." Proceedings of the Institution of Mechanical Engineers. Part H, Journal of engineering in medicine. **207**(H3): 139-148.

Chang, Y.-W., F.-C. Su, H.-W. Wu and K.-N. An (1999). "Optimum length of muscle contraction." Clinical Biomechanics Clinical Biomechanics **14**(8): 537-542.

Crowninshield, R. D. (1978). "Use of Optimization Techniques to Predict Muscle Forces." J Biomech Eng Journal of Biomechanical Engineering **100**(2): 88.

Delp, S. L., F. C. Anderson, A. S. Arnold, P. Loan, A. Habib, C. T. John, E. Guendelman and D. G. Thelen (2007). "OpenSim: Open-Source Software to Create and Analyze Dynamic Simulations of Movement." Biomedical Engineering, IEEE Transactions on **54**(11): 1940-1950.

Dwyer-Lindgren, L., G. Freedman, R. E. Engell, T. D. Fleming, S. S. Lim, C. Murray and A. H. Mokdad (2013). "Prevalence of physical activity and obesity in US counties, 2001-2011: a road map for action." Popul Health Metr **11**(1): 7.

Escamilla, R., N. Zheng, T. Macleod, W. Brent Edwards, R. Imamura, A. Hreljac, G. Fleisig, K. Wilk, C. Moorman and J. Andrews (2009). "Patellofemoral joint force and stress during the wall squat and one-leg squat." Medicine+ Science in Sports+ Exercise **41**(4): 879.

Escamilla, R. F., G. S. Fleisig, N. Zheng, J. E. Lander, S. W. Barrentine, J. R. Andrews, B. W. Bergemann and C. T. Moorman (2001). "Effects of technique variations on knee biomechanics during the squat and leg press." Medicine and science in sports and exercise **33**(9): 1552-1566.

Gordon, A. M., A. F. Huxley and F. J. Julian (1966). "The variation in isometric tension with sarcomere length in vertebrate muscle fibres." The Journal of Physiology **184**(1): 170-192.

Hamill, J. and K. Knutzen (2009). Biomechanical basis of human movement. Philadelphia, Wolters Kluwer Health/Lippincott Williams and Wilkins.

Harman, E. (1983). "Resistive Torque Analysis of 5 Nautilus Exercise MACHINES." Medicine & Science in Sports & Exercise **15**(2): 113.

Herzog, W. (1987). "Individual muscle force estimations using a non-linear optimal design." Journal of Neuroscience Methods **21**(2): 167-179.

Hill, A. (1938). "The heat of shortening and the dynamic constants of muscle." Proceedings of the Royal Society of London B: Biological Sciences **126**(843): 136-195.

Holzbaur, K., W. Murray and S. Delp (2005). "A Model of the Upper Extremity for Simulating Musculoskeletal Surgery and Analyzing Neuromuscular Control." Annals of Biomedical Engineering **33**(6): 829-840.

Holzbaur, K. R. S., W. M. Murray, G. E. Gold and S. L. Delp (2007). "Upper limb muscle volumes in adult subjects." Journal of Biomechanics **40**(4): 742-749.

Kaufman, K. R., K. W. An, W. J. Litchy and E. Y. Chao (1991). "Physiological prediction of muscle forces--I. Theoretical formulation." Neuroscience **40**(3): 781-792.

Lemay, M. A. and P. E. Crago (1996). "A dynamic model for simulating movements of the elbow, forearm, and wrist." Journal of Biomechanics **29**(10): 1319-1330.

Li, G., J. E. Pierce and J. H. Herndon (2006). "A global optimization method for prediction of muscle forces of human musculoskeletal system." BM Journal of Biomechanics **39**(3): 522-529.

Millard, M., T. Uchida, A. Seth and S. L. Delp (2013). "Flexing computational muscle: modeling and simulation of musculotendon dynamics." Journal of biomechanical engineering **135**(2).

Murray, W. M., T. S. Buchanan and S. L. Delp (2000). "The isometric functional capacity of muscles that cross the elbow." Journal of Biomechanics **33**(8): 943-952.

Neumann, D. A. (2002). Kinesiology of the musculoskeletal system foundations for physical rehabilitation. St. Louis, Mosby.

Pauly, J. E., J. L. Rushing and L. E. Scheving (1967). "An electromyographic study of some muscles crossing the elbow joint." The Anatomical Record **159**(1): 47-53.

Pigeon, P., L. H. Yahia and A. G. Feldman (1996). "Moment arms and lengths of human upper limb muscles as functions of joint angles." Journal of Biomechanics Journal of Biomechanics **29**(10): 1365-1370.

Pontonnier, C. and G. Dumont (2009). "Inverse dynamics method using optimization techniques for the estimation of muscles forces involved in the elbow motion." International Journal on Interactive Design and Manufacturing (IJIDeM) **3**(4): 227-236.

Raikova, R. (1996). "A model of the flexion-extension motion in the elbow joint some problems concerning muscle forces modelling and computation." Journal of biomechanics **29**(6): 763-772.

Saul, K. R., X. Hu, C. M. Goehler, M. E. Vidt, M. Daly, A. Velisar and W. M. Murray (2014). "Benchmarking of dynamic simulation predictions in two software platforms using an upper limb musculoskeletal model." Computer Methods in Biomechanics and Biomedical Engineering **18**(13): 1445-1458.

Wilkie, D. (1949). "The relation between force and velocity in human muscle." The Journal of physiology **110**(3-4): 249-280.

Woittiez, R. D., P. A. Huijing, H. B. K. Boom and R. H. Rozendal (1984). "A three-dimensional muscle model: A quantified relation between form and function of skeletal muscles." JMOR Journal of Morphology **182**(1): 95-113.

Zajac, F. E. and M. E. Gordon (1989). "Determining muscle's force and action in multi-articular movement." Exercise and sport sciences reviews **17**: 187-230.

Zheng, N., S. W. Barrentine, G. S. Fleisig and J. R. Andrews (2008). "Kinematic Analysis of Swing in Pro and Amateur Golfers." Int J Sports Med **29**(06): 487-493.